

RIA-81-U91

MHSMP-80-20

TECHNICAL
LIBRARY

Dist. Category UC-45

TOOL FORCE EVALUATION OF LATHE MACHINED
HIGH EXPLOSIVES

Gary L. Flowers

DEVELOPMENT DIVISION

April 1980

DISSEMINATION STATEMENT
Approved for public release
Distribution Unlimited

Process Development
Endeavor No. 302

19970805 117

DTIC QUALITY INSPECTED 3



Mason & Hanger-Silas Mason Co., Inc.
Partex Plant

OPERATED FOR THE
Department of Energy

UNDER
U. S. GOVERNMENT CONTRACT DE-AC04-76DP-00487

P. O. BOX 30020
AMARILLO, TEXAS 79177
806-335-1581

NOTICE

This report was prepared as an account of work sponsored by the United States Government. Neither the United States nor the United States Department of Energy, nor their employees, nor any of their contractors, subcontractors, or their employees, makes any warranty, express or implied, or assumes any legal liability or responsibility for the accuracy, completeness or usefulness of any information, apparatus, product or process disclosed, or represents that its use would not infringe privately-owned rights.

Printed in the United States of America
Available from

National Technical Information Service

U. S. Department of Commerce

5285 Port Royal Road

Springfield, VA 22161

Price: Printed Copy \$6.00 ; Microfiche ^{3.50}~~\$3.00~~

TOOL FORCE EVALUATION OF LATHE MACHINED HIGH EXPLOSIVES

Gary L. Flowers

DEVELOPMENT DIVISION
(April 1980)

Process Development
Endeavor No. 302

ABSTRACT

The purpose of this study was to develop a better understanding of the effects of machining properties upon tool forces encountered during lathe machining of high explosives, in order to optimize machining conditions for mechanical properties test specimens. Monetary considerations dictated that the tooling either already exist or be fabricated in-house using limited machine shop capability. The design chosen which fit between the tool holder and the tool post and interfaced to existing signal conditioners was easily fabricated. The study evaluated all forces on the cutter during machining of two types of high explosives at four cutter radii, four feed rates, three depths of cut and two cutting speeds.

The study pointed out design problems, instrumentation drift, tool chatter and detection levels. It also showed that the type of high explosive was more significant than first thought toward influencing tool force levels.

INTRODUCTION

With the spiraling cost of labor and materials coupled with the stringent safety requirements involving the machining of high explosives, safer and more efficient machining conditions must be found. In an effort to move in this direction, a study was undertaken to better understand the effect of various machining parameters with the forces exerted upon the cutting tool during lathe machining operations. This tool force study, while only a beginning, demonstrated the type of tooling required, signal levels to be anticipated, some of the problems associated with setup, calibration, data reduction, etc., and the overall feasibility of on-line measurement of tool forces during machining operations.

The experiment was designed as a six variable complete block matrix. These six variables, along with the specific values for each of them are as follows:

- Type of High Explosive -- LX-10 (95% HMX/5% Viton),
RX-03-BB (92.5% TATB/7.5% Kel-F)
- Cutter Radius -- 0.005, 0.030, 0.100, 0.250 inch
- Feed Rate -- 0.003, 0.012, 0.024, 0.0336 inch/revolution
- Depth of Cut -- 0.020, 0.100, 0.250 inch
- Cutter Attack Angle -- 0, 30, 45 degrees
- Cutting Speed -- Near 210, Near 75 SFM (surface feet per minute)

Since virtually all machines in use today still employ the English dimensioning system, this report will be written in this system to facilitate correlation of data with current machining practices.

DISCUSSION

THEORY AND DESIGN

The equipment for tool force measuring had to be relatively inexpensive and either already in existence or capable of being fabricated in-house. In addition, the transducer(s) had to mount between the existing tool post holder and cutter holder without changing the height of the cutter or adding excessively to the overall tool setup dimension. Several designs were considered with the one in Fig. 1 being selected. This design allowed fabrication of the two steel sensor arms (Fig. 2), installation of the strain gages and insertion of these arms between the tool post holder and the cutter holder.

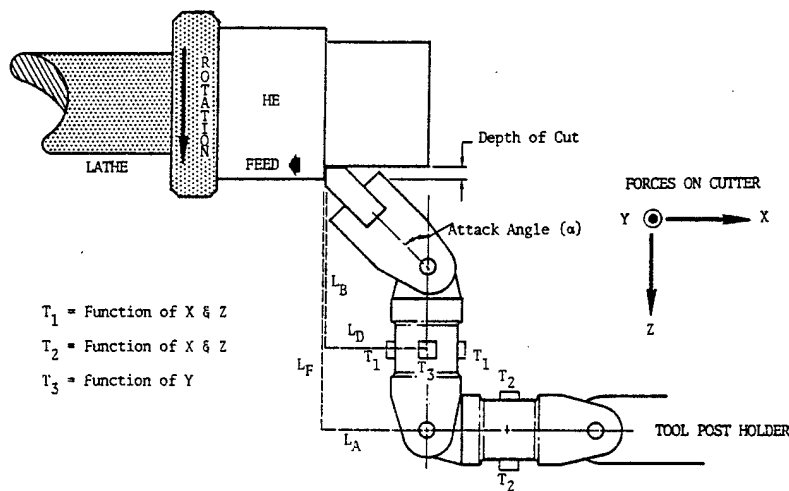


Fig. 1. Tool Force Measurement Setup for Lathe Machining

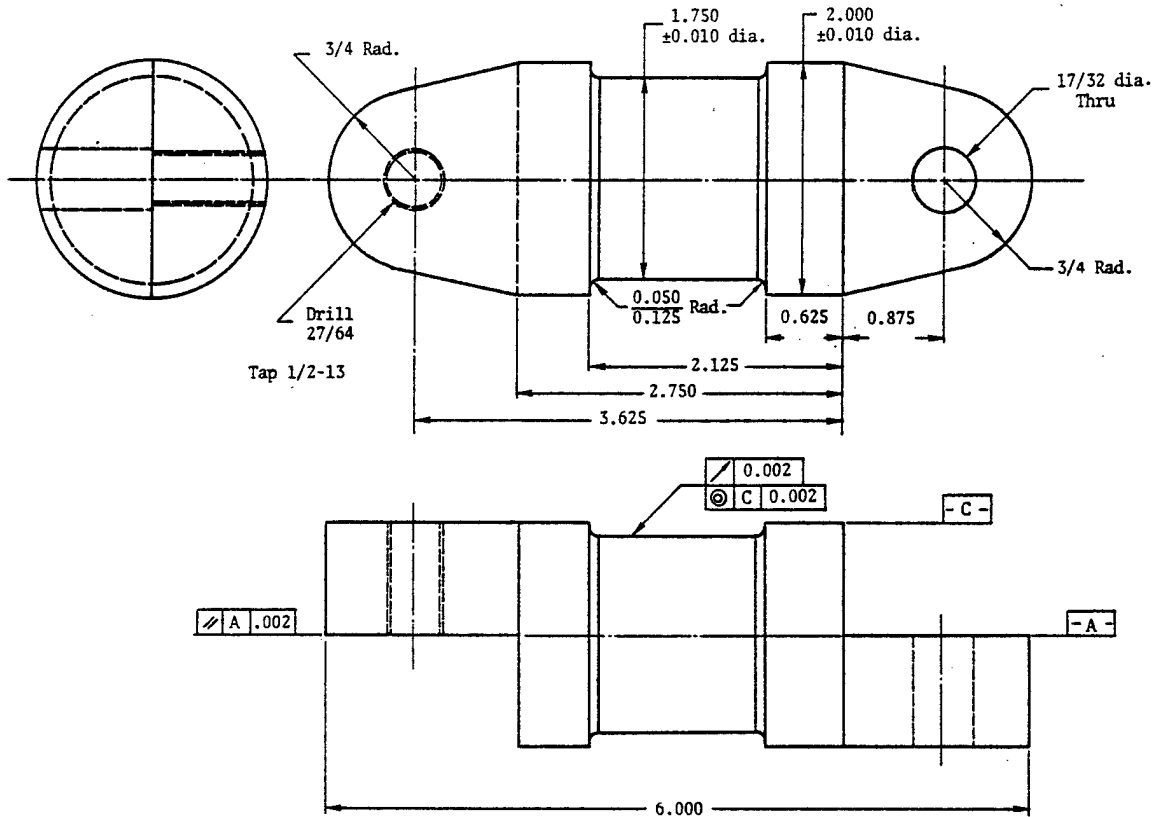


Fig. 2. Tool Force Transducer Sensor Arm

This design employs three pairs of semi-conductor strain gages identified in Fig. 1 as T_1 , T_2 and T_3 . As can readily be seen in the figure, T_3 is a function only of forces in the Y direction, whereas T_1 and T_2 are each functions of X and Z. By knowing the moment arm lengths (L_A , L_B , L_D and L_F) through which these forces act, it is possible to calculate the X, Y, and Z forces exerted on a cutter during machining.

The strain gages employed were SR-4 semi-conductor gages manufactured by BLH Electronics of Waltham, Mass. The gage type was SPB3-12-12. The gages used were single element gages with a nominal backed resistance (R_0) of 119 Ω and a nominal gage factor^a of 119. Two gages in a half bridge (see Fig. 3) were employed to measure the bending moments shown in Fig. 1. Bending torques of as little as 1.0 in-lb can be measured with the 1-3/4 inch diameter steel transducers before noise becomes a significant problem.

^aGage Factor = $\left(\frac{R}{R_0}\right)$ at a tensile strain of 500 $\mu\text{in/in}$.

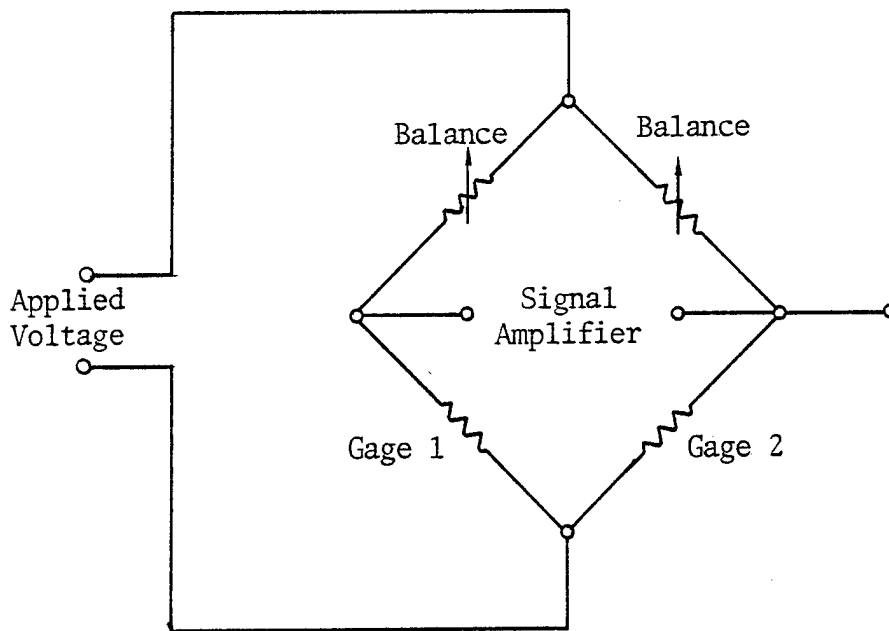


Fig. 3. Strain Gage Electrical Bridge

The basic cutter employed at Pantex for high explosive machining is a carbide tipped design as detailed in Fig. 4. The 7° relief angle coupled with the flat top of the cutter actually makes this a "scraper" rather than a "cutter." Tool forces could be minimized even further if a sharp cutter were employed, but this was not considered in the study. The 7° relief angle also puts another restriction on the system. To prevent dragging of the explosive on the 7° relief face, there is a critical relationship between feed rate and cutting speed. The point at which dragging will occur can be defined as:

$$\tan(\text{relief angle}) = \frac{(F)(S)}{\pi(D)(S)} = \frac{F}{\pi D}$$

where,

F = Feed rate (inch/revolution)

S = Speed (RPM)

D = Piece diameter (inches)

If one arbitrarily chooses the worst case feed rate of 0.035 inch/revolution, then one can plot the minimum allowable diameter (below which dragging will occur) as a function of cutter relief angle (see Fig. 5). Since the nominal cutter relief angle used at Pantex is 7°, Fig. 5 easily shows that even allowing substantial deviations from this, the critical diameter is still very small and therefore dragging of a cutter due to relief angle should never occur.

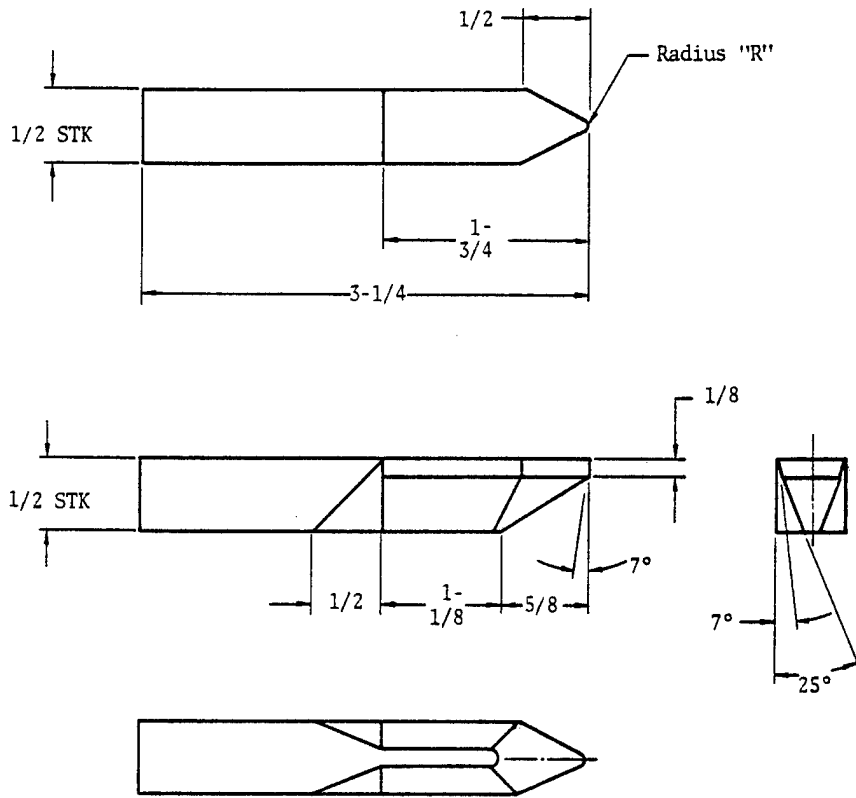


Fig. 4. Typical Cutter

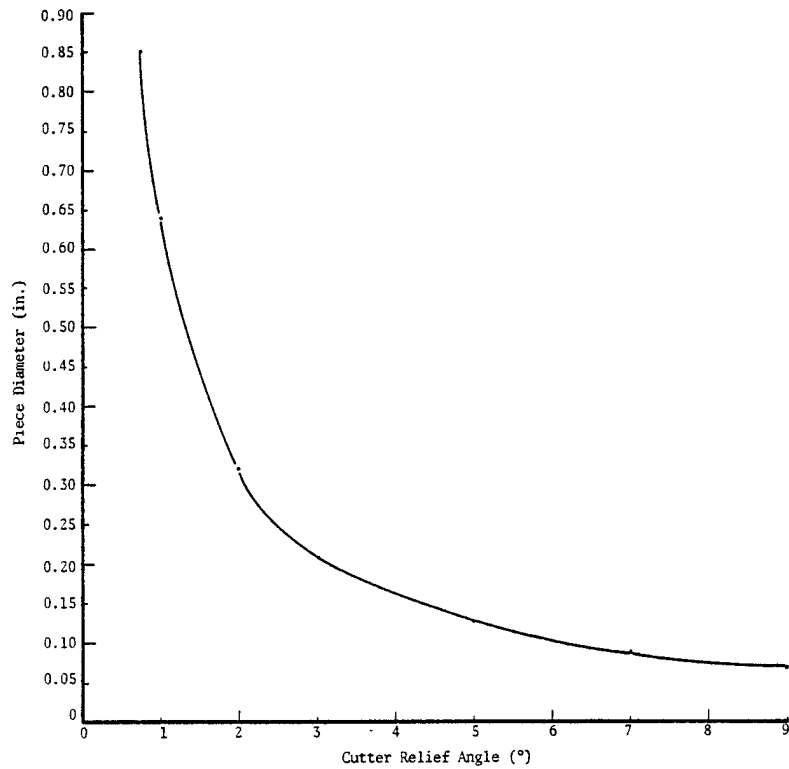


Fig. 5. Minimum Diameter to Induce Drag vs. Cutter Relief Angle (0.035 inch/revolution Feed Rate)

SETUP AND OPERATION

The recessed areas of the transducer arms were potted with a silicone potting compound (Sylgard 184)^b to reduce the potential of handling damage and the effect of temperature on bridge balance. Signal drift due to cooling water and ambient temperature changes as well as instrumentation drift was present throughout the experiment. However, while the signal output could easily be reset to zero prior to each test run, this nuisance could present a significant problem for other applications and would therefore require additional work to resolve.

Calibration of the system involves knowing the moment arm lengths very accurately and insuring that the angular relationship among components is maintained accurately. This task proved to be considerably more difficult than was first anticipated and was eventually responsible for the loss of some data. Calibration was accomplished on the lathe with $\alpha = 0$ and a special cutter in place allowing dead weights to be applied via a pulley system.

During machining, water was used as the coolant. A tailstock was used to minimize sample deflection during machining.

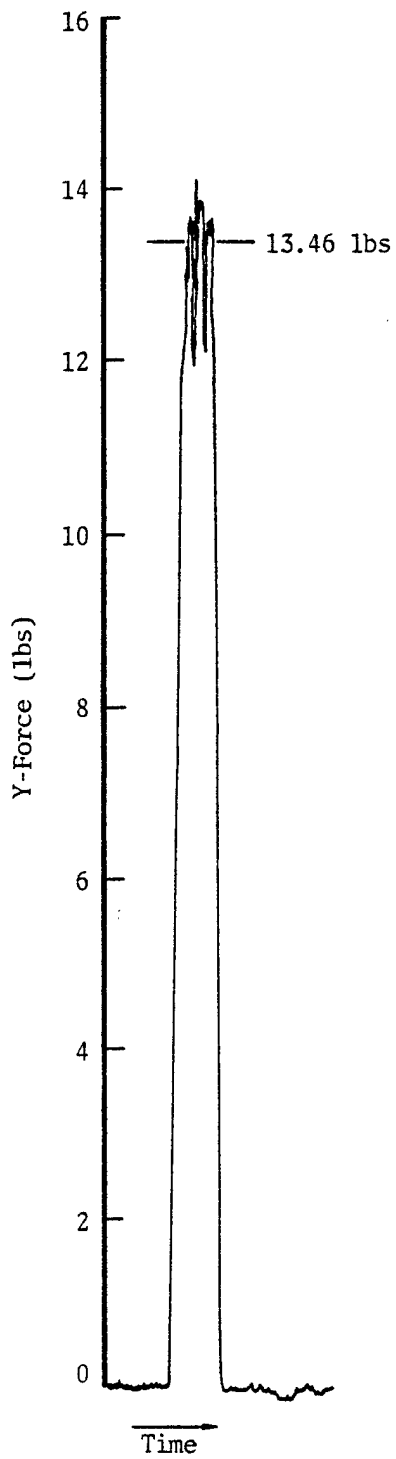
In an effort to minimize the amount of explosive machined away during testing and since the lathe on which testing was done is a specific, selectable RPM machine, the cutting rate in terms of surface feet/minute (SFM) could not be maintained constant. Using the available RPM selectors, the cutting rate was maintained as close to 75 SFM and as close but below 210 SFM as possible. As an example, for the RX-03-BB machining, the cutting rates varied from 75.6 to 85.2 and from 138 to 158 SFM. For 160 test points, the 7.750 inch diameter by 6.750 inch long billet was machined down to a diameter of 7.00 inches.

Tool chatter and electronic noise were somewhat of a problem in being able to interpret the strip chart records of the transducers accurately. Fig. 6 shows two typical T_3 transducer (Y force) records for RX-03-BB. Fig. 6A is the record for a 0.100-inch radius cutter machining a 0.250-inch deep cut at 0.0336-inch/revolution cutting rate. Notice the minimal noise level at zero load compared to the 2-pound load variation during machining. Fig. 6B is the record for a 0.100-inch radius cutter machining a 0.020-inch deep cut at 0.024 inch/revolution cutting rate. The noise sensitivity was high but the signal variation during machining was low. In all cases, the signal was read at the average value.

DATA REDUCTION

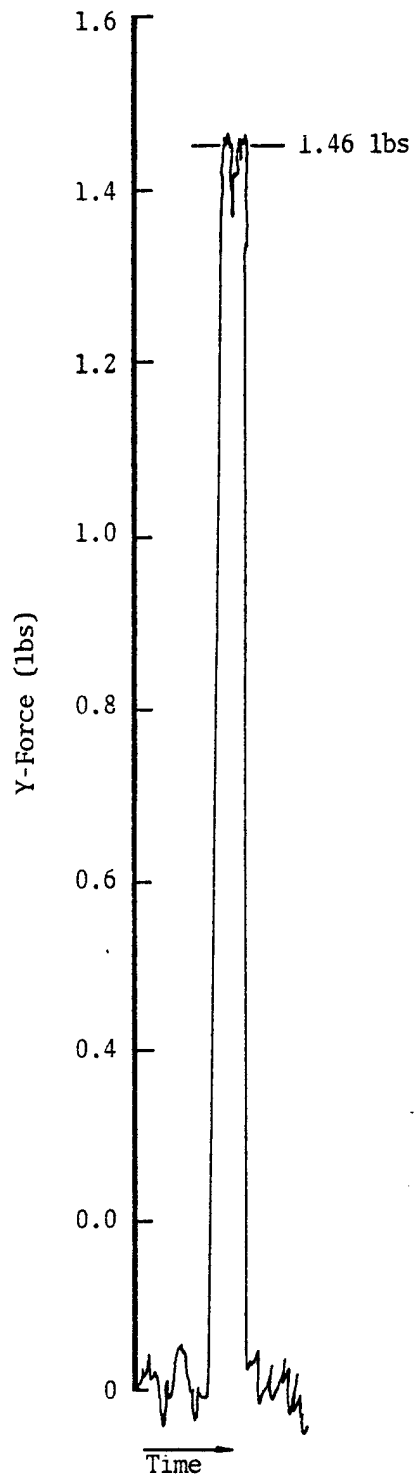
As can be seen from Fig. 1, the forces exerted on the cutter during machining exert bending moments on the three pairs of strain gages. By measuring the bending strain on each pair of strain gages and by knowing the distances through which the forces were applied, the forces can be readily calculated.

^bProduct of Dow Corning, Midland, Michigan.



0.100" Radius,
 0.0336"/rev,
 0.250" depth,
 154 SFM

6A



0.100" Radius,
 0.024"/rev,
 0.020" depth,
 82 SFM

6B

Fig. 6. Typical Transducer Strip Chart Outputs
 For Heavy Cut and Light Cut on RX-03-BB

$$\text{Torque } T_1 = L_B(F_X) - L_D(F_Z) = (T_1 \text{ chart}) (T_1 \text{ calibration factor})$$

$$\text{Torque } T_2 = L_A(F_Z) - L_F(F_X) = (T_2 \text{ chart}) (T_2 \text{ calibration factor})$$

$$\text{Torque } T_3 = L_B(F_Y) = (T_3 \text{ chart}) (T_3 \text{ calibration factor})$$

or,

$$F_X = \frac{T_1(L_A) + T_2(L_D)}{(L_A)(L_B) - (L_F)(L_D)}$$

$$F_Y = \frac{T_3}{L_B}$$

$$F_Z = \frac{T_1(L_F) + T_2(L_B)}{(L_A)(L_B) - (L_F)(L_D)}$$

In order to insure that the equations for T_1 and T_2 remain independent simultaneous equations, $(L_A)(L_B)$ must not equal $(L_F)(L_D)$.

EFFECT OF CALIBRATION WEIGHT ERROR

Forces of $F_X = + 10$, $F_Y = + 10$ and $F_Z = 0$ pounds were used to calibrate T_1 , T_2 and T_3 . The error in being able to apply the weight due to a non-frictionless pulley system for T_1 and T_2 calibration was estimated at ± 0.1 pounds or $\pm 1\%$. The calibration factors for T_1 and T_2 can be calculated by:

$$T_1 \text{ cal} = \frac{(F_X) (T_1 \text{ moment arm})}{T_1 \text{ chart reading}}$$

$$T_2 \text{ cal} = \frac{(F_X) (T_2 \text{ moment arm})}{T_2 \text{ chart reading}}$$

A $\pm 1\%$ error in F_X results in a $\pm 1\%$ error in both $T_1 \text{ cal}$ and $T_2 \text{ cal}$.

Solving for the actual F_X and F_Z errors at various attack angles and dividing them by the corresponding F_X and F_Z true values yields the following:

- A $\pm 1\%$ calibration weight error yields
- $\pm 1\%$ F_X error at $\alpha = 0$
- $\pm 2\%$ F_X error at all other angles
- $\pm 2\%$ F_Z error at all angles

There are many other error possibilities in the system which will be mentioned but not discussed due to the complex interaction of these errors. A Monte Carlo analysis technique could be employed if a better understanding is desired.

1. Moment arm lengths
2. Attack angle
3. Transducer 1 location relative to coordinate axis
4. Transducer 2 location relative to coordinate axis
5. Sensitivity drift
6. Linearity of sensitivity
7. Effect of cutter chatter
8. Electrical noise

Data were gathered for LX-10 at attack angle of 0, 30, 45 and 60°. Subsequent data reduction showed large variations in F_X and F_Z values for 45 and 60° data sets. This is explained by the relationship the moment arms at these angles had on the reduction equations, where very small errors had very large effects on the calculated forces. As a result, only the 0 and 30° data sets were planned to be used. The attack angles 0 and 30° were then used for RX-03-BB machining. It was during the RX-03-BB machining series that an unexplainable problem became evident in the separation of the F_X and F_Z forces, especially at attack angles other than 0°. Non-real forces for both F_X and F_Z were encountered (example: decreasing F_X and increasing negative F_Z as feed rate increases). An exhaustive study and post test calibration failed to locate the cause of this problem but did point to the problem occurring to a lesser degree on the LX-10 data sets.

Under certain machining conditions, all three forces should be the same regardless of attack angle. For example, a 0.250-inch radius cutter presents the same cutter profile to the explosive during machining at 0° as it does at 30° for cuts less than 0.250-inch deep. While F_Y agrees with this for both LX-10 and RX-03-BB, F_X and F_Z do not. As a result, all non-0° F_X and F_Z data are suspect and are not reported. Since at 0°, all F_X 's are functions of T_1 only and since T_1 was calibrated at 0°, these F_X 's are believed to be accurate. F_Z for RX-03-BB is known to be erroneous in all cases and are not reported. F_Z for LX-10 is reported for 0° but should be used with caution. These data are displayed graphically in the Appendix.

CONCLUSIONS

For the transducer used in this experiment, the design is inadequate to allow accurate force vector separation at all reasonable attack angles.

The design of holding fixtures for the explosive charge during machining depends very heavily on the type of material to be machined since the forces change dramatically with the type of explosive. For example, at low feed rates, the F_x force to machine LX-10 is 20 to 30% greater than for RX-03-BB, while at high feed rates, the difference is 200 to 300%. For the F_y forces, the figures differ by over 100% in all cases.

The slower the RPM, the greater the forces on the cutter. This effect becomes very pronounced as the feed rate is also increased.

For a given set of machining conditions, the F_x and F_y forces are essentially independent of cutter radius.

RECOMMENDATIONS

- To minimize signal drift due to instrumentation and temperature, additional work would be required to allow equipment to be used in a production environment.
- In situ calibration should be designed into the next generation transducer.
- The transducer should be redesigned and/or a commercially-available dynamometer be evaluated to eliminate force interaction and separation problems.
- A computer model should be prepared which would allow force predictions for any reasonable set of operating conditions for any explosive based upon a few measured points for that material.

APPENDIX

Figure

Title

| Figure | Title |
|--------|-------------------------------------------------------------------|
| A-1 | F_X vs. Depth of Cut for LX-10 with 0.005 inch Radius Cutter |
| A-2 | F_X vs. Depth of Cut for LX-10 with 0.030 inch Radius Cutter |
| A-3 | F_X vs. Depth of Cut for LX-10 with 0.100 inch Radius Cutter |
| A-4 | F_X vs. Depth of Cut for LX-10 with 0.250 inch Radius Cutter |
| A-5 | F_Y vs. Depth of cut for LX-10 with 0.005 inch Radius Cutter |
| A-6 | F_Y vs. Depth of Cut for LX-10 with 0.030 inch Radius Cutter |
| A-7 | F_Y vs. Depth of Cut for LX-10 with 0.100 inch Radius Cutter |
| A-8 | F_Y vs. Depth of Cut for LX-10 with 0.250 inch Radius Cutter |
| A-9 | F_Z vs. Depth of Cut for LX-10 with 0.005 inch Radius Cutter |
| A-10 | F_Z vs. Depth of Cut for LX-10 with 0.030 inch Radius Cutter |
| A-11 | F_Z vs. Depth of Cut for LX-10 with 0.100 inch Radius Cutter |
| A-12 | F_Z vs. Depth of Cut for LX-10 with 0.250 inch Radius Cutter |
| A-13 | F_X vs. Cutter Radius for LX-10 at Different Cutting Depths |
| A-14 | F_Y vs. Cutter Radius for LX-10 at Different Cutting Depths |
| A-15 | F_Z vs. Cutter Radius for LX-10 at Different Cutting Depths |
| A-16 | F_X vs. Feed Rate for LX-10 at Various Cutter Radii |
| A-17 | F_Y vs. Feed Rate for LX-10 at Various Cutter Radii |
| A-18 | F_X vs. Depth of Cut for RX-03-BB with 0.005 inch Radius Cutter |
| A-19 | F_X vs. Depth of Cut for RX-03-BB with 0.030 inch Radius Cutter |
| A-20 | F_X vs. Depth of Cut for RX-03-BB with 0.100 inch Radius Cutter |
| A-21 | F_X vs. Depth of Cut for RX-03-BB with 0.250 inch Radius Cutter |
| A-22 | F_Y vs. Depth of Cut for RX-03-BB with 0.005 inch Radius Cutter |
| A-23 | F_Y vs. Depth of Cut for RX-03-BB with 0.030 inch Radius Cutter |
| A-24 | F_Y vs. Depth of Cut for RX-03-BB with 0.100 inch Radius Cutter |
| A-25 | F_Y vs. Depth of Cut for RX-03-BB with 0.250 inch Radius Cutter |
| A-26 | F_X vs. Cutter Radius for RX-03-BB at Different Cutting Depths |
| A-27 | F_Y vs. Cutter Radius for RX-03-BB at Different Cutting Depths |
| A-28 | F_X vs. Feed Rate for RX-03-BB at Various Cutter Radii |
| A-29 | F_Y vs. Feed Rate for RX-03-BB at Various Cutter Radii |

LX-10 TOOL FORCE STUDY F_X VS DEPTH OF CUT
 CUTTER RADIUS = 0.005 INCH, ATTACK ANGLE = 0 DEGREES
 X .0336 IPA F Δ .0240 IPA F + .0120 IPA F X .0030 IPA F \diamond .0030 IPA S
 ∇ .0120 IPA S \square .0240 IPA S Y .0336 IPA S

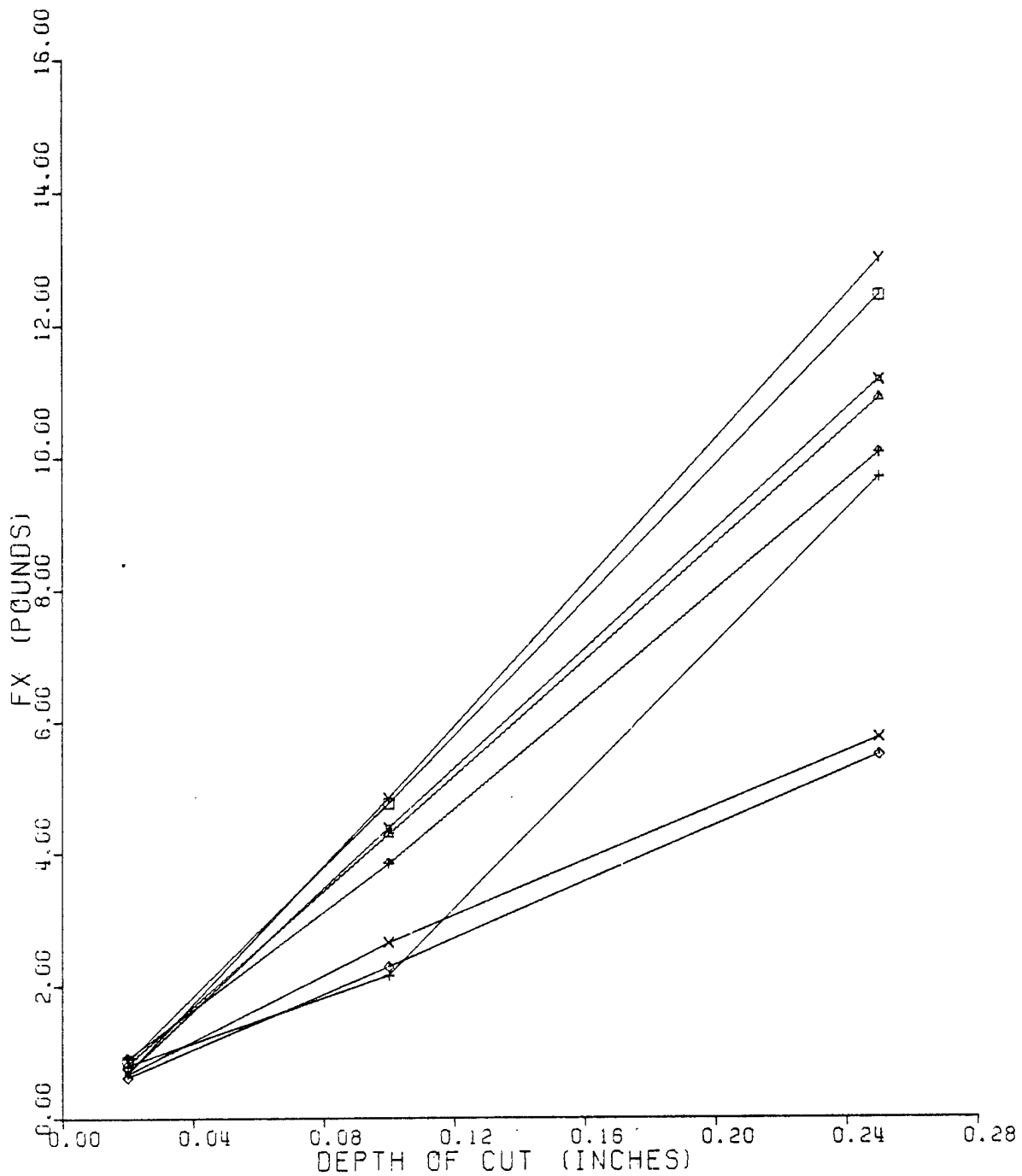


Fig. A-1. F_X vs. Depth of Cut for LX-10 with 0.005 inch Radius Cutter

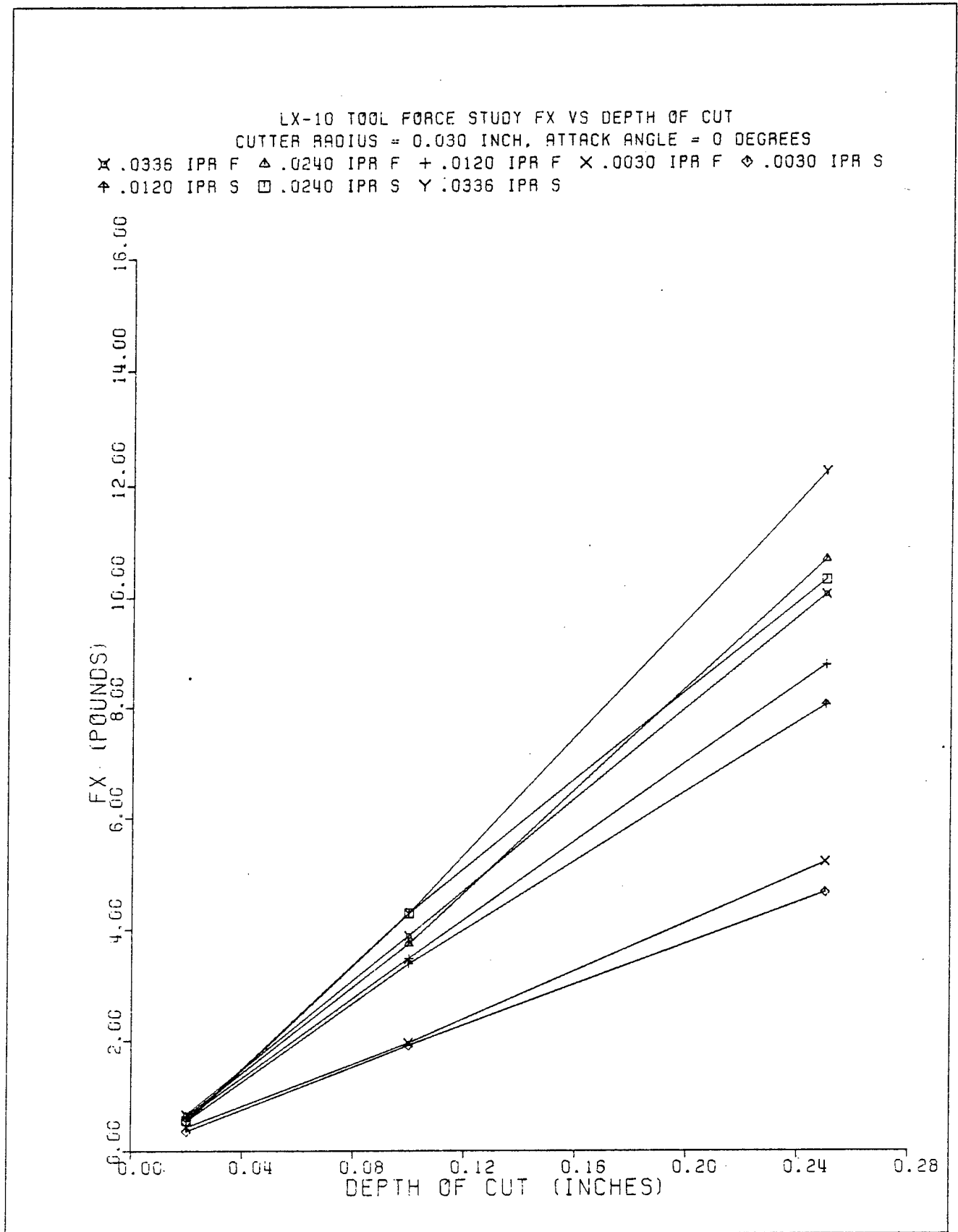


Fig. A-2. F_X vs. Depth of Cut for LX-10 with 0.030 inch Radius Cutter

LX-10 TOOL FORCE STUDY F_X VS DEPTH OF CUT
 CUTTER RADIUS = 0.100 INCH, ATTACK ANGLE = 0 DEGREES
 X .0336 IPR F Δ .0240 IPR F + .0120 IPR F X .0030 IPR F ◇ .0030 IPR S
 † .0120 IPR S □ .0240 IPR S Y .0336 IPR S

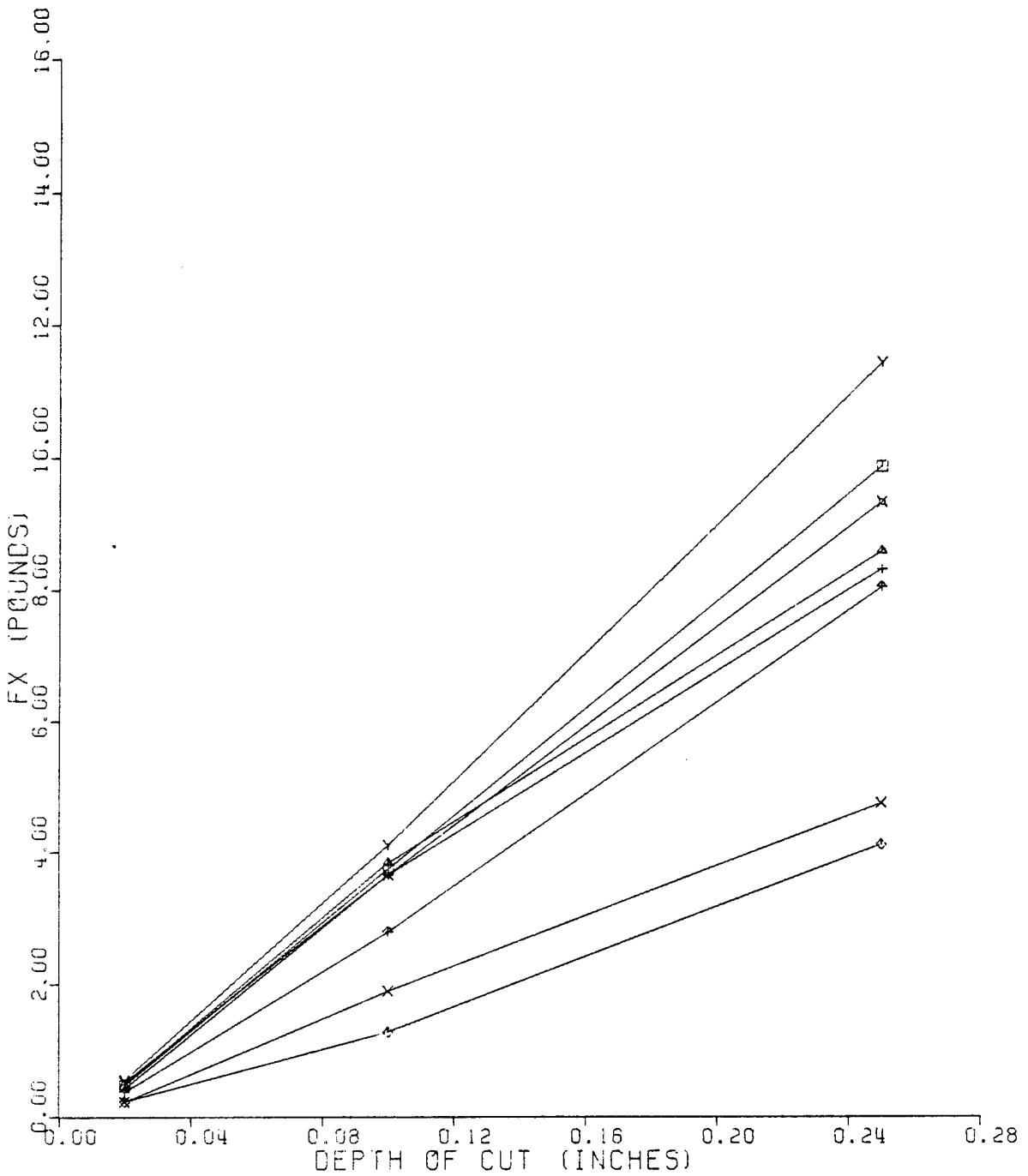


Fig. A-3. F_X vs. Depth of Cut for LX-10 with 0.100 inch Radius Cutter

LX-10 TOOL FORCE STUDY F_X VS DEPTH OF CUT
 CUTTER RADIUS = 0.250 INCH. ATTACK ANGLE = 0 DEGREES
 * .0336 IPR F \blacktriangle .0240 IPR F + .0120 IPR F \times .0030 IPR F \diamond .0030 IPR S
 \blacktriangleright .0120 IPR S \square .0240 IPR S γ .0336 IPR S

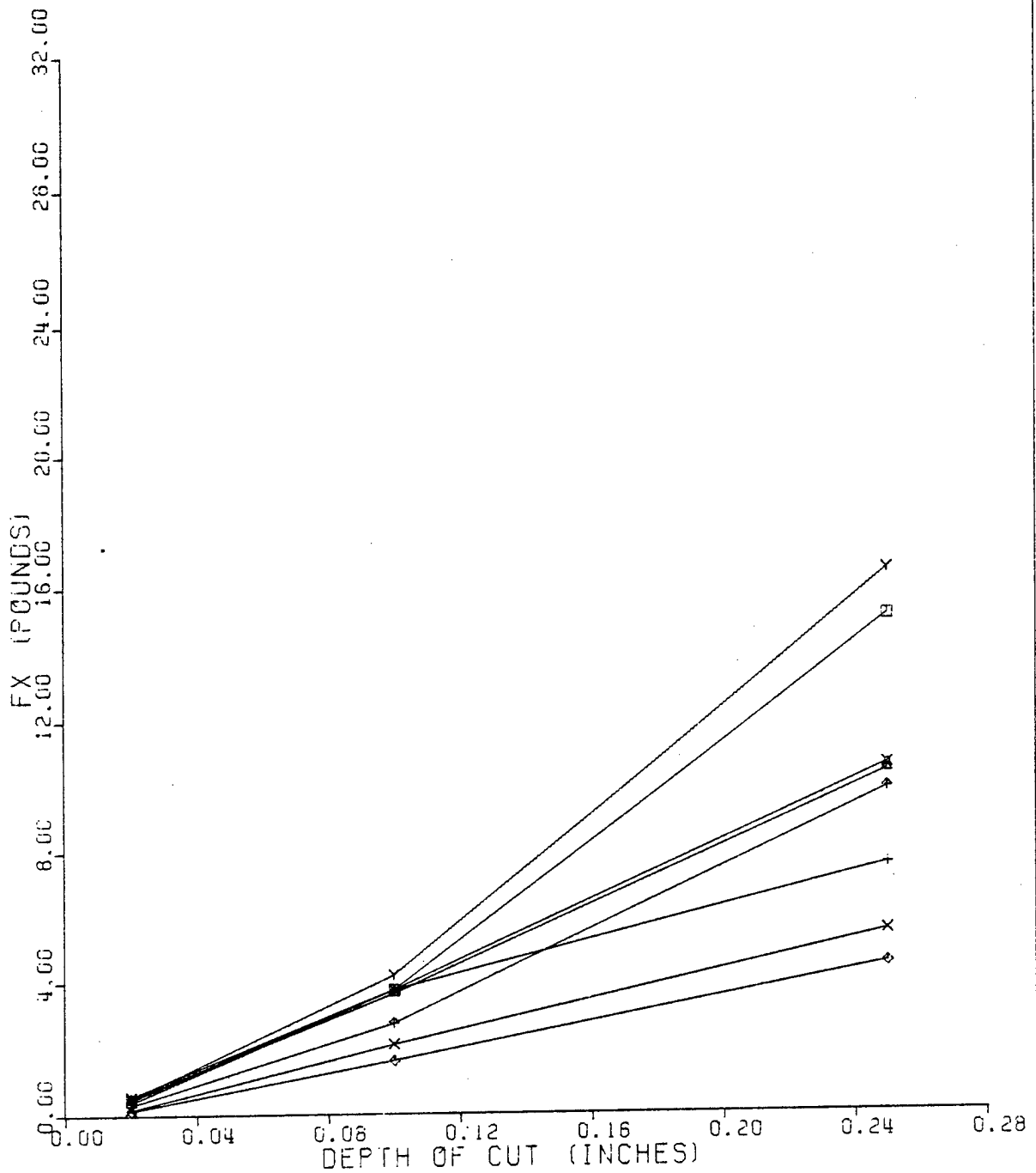


Fig. A-4. F_X vs. Depth of Cut for LX-10 with 0.250 inch Radius Cutter

LX-10 TOOL FORCE STUDY F_Y VS DEPTH OF CUT
 CUTTER RADIUS = 0.005 INCH, ATTACK ANGLE = 0 DEGREES
 * .0336 IPA F Δ .0240 IPA F + .0120 IPA F \times .0030 IPA F \diamond .0030 IPA S
 ∇ .0120 IPA S \square .0240 IPA S Y .0336 IPR S

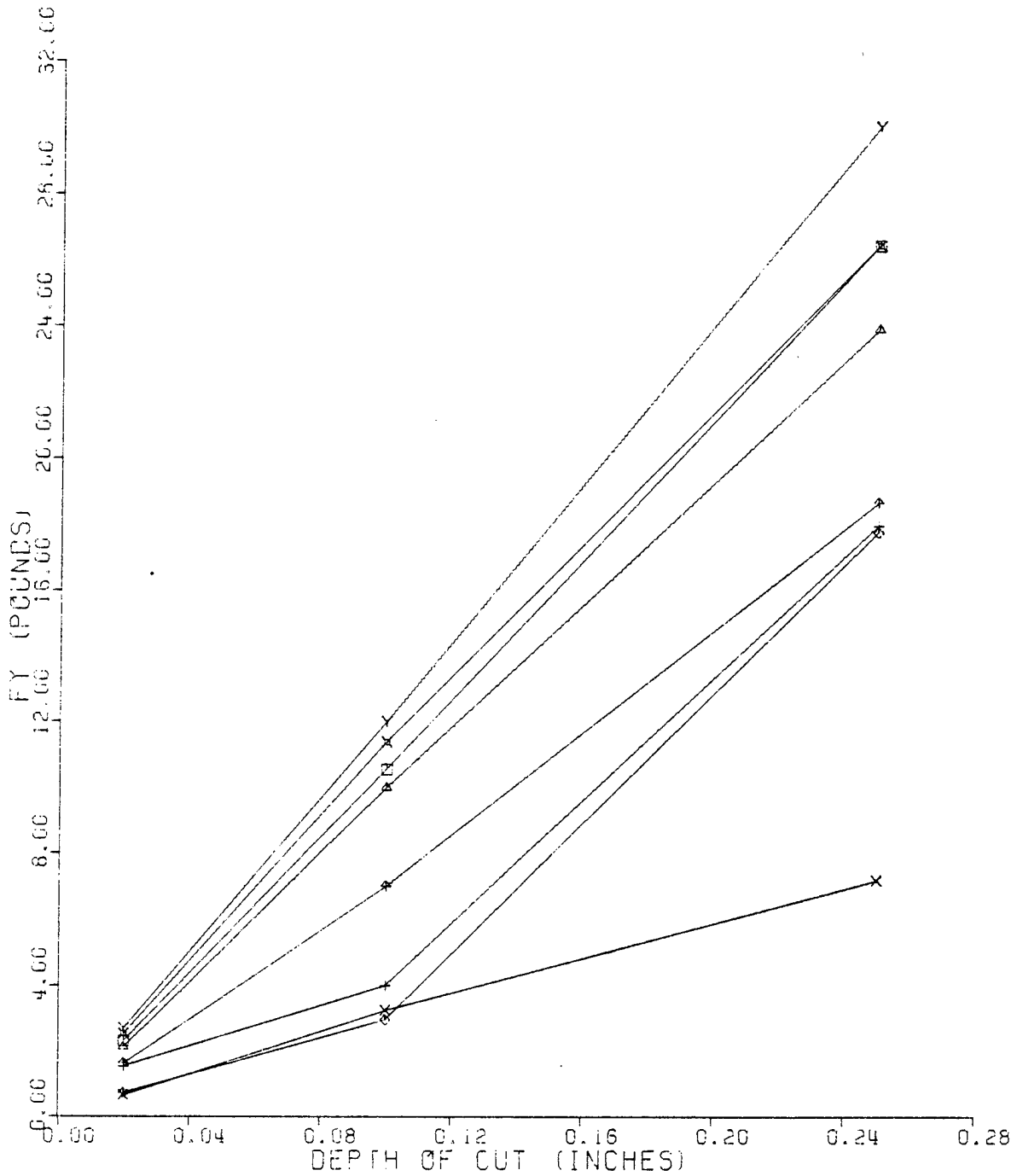


Fig. A-5. F_Y vs. Depth of Cut for LX-10 with 0.005 inch Radius Cutter

LX-10 TOOL FORCE STUDY F_Y VS DEPTH OF CUT
 CUTTER RADIUS = 0.030 INCH, ATTACK ANGLE = 0 DEGREES
 ✕ .0336 IPR F △ .0240 IPR F + .0120 IPR F ✕ .0030 IPR F ◇ .0030 IPR S
 † .0120 IPR S □ .0240 IPR S † .0336 IPR S

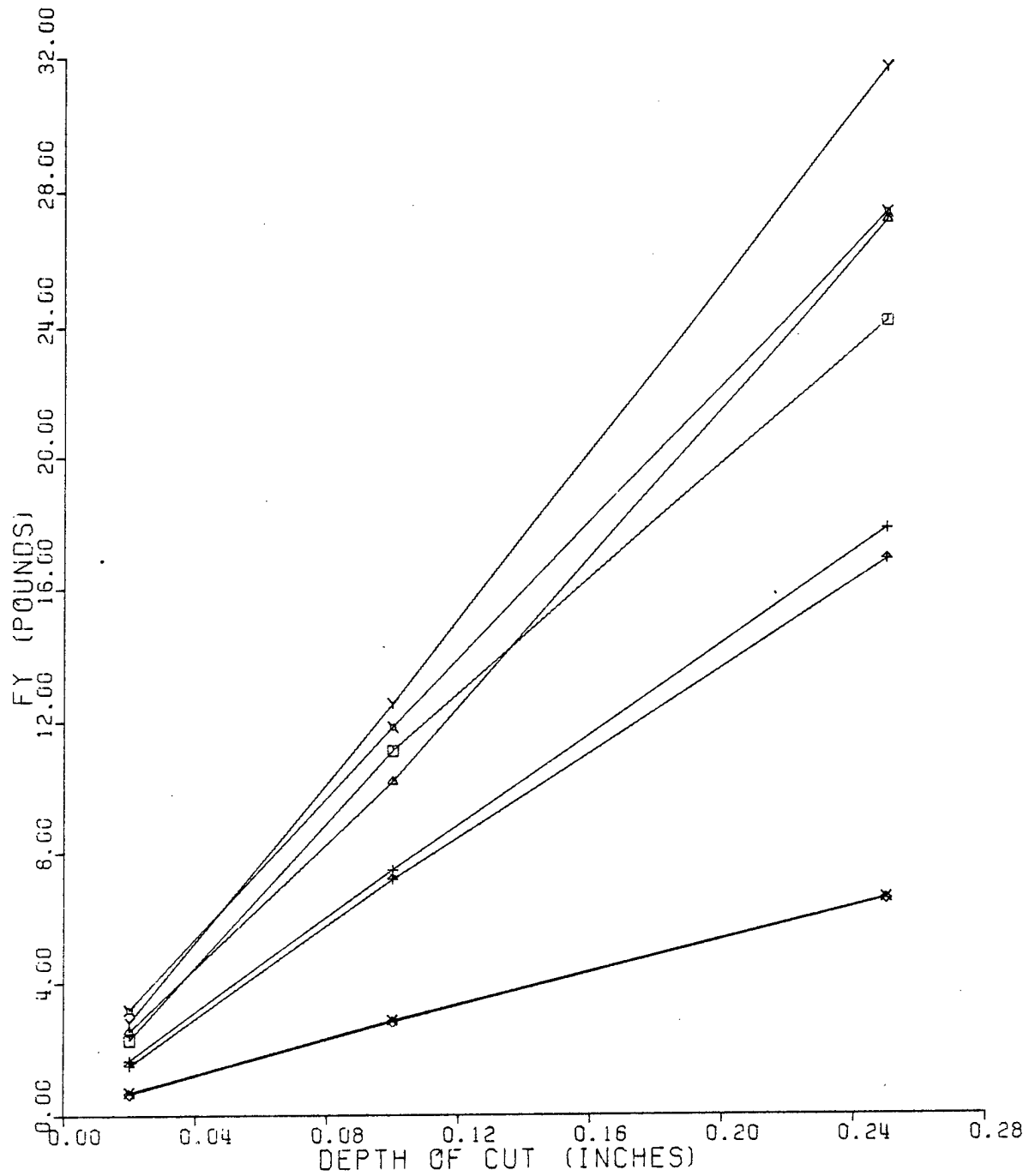


Fig. A-6. F_Y vs. Depth of Cut for LX-10 with 0.030 inch Radius Cutter

LX-10 TOOL FORCE STUDY F_Y VS DEPTH OF CUT
 CUTTER RADIUS = 0.100 INCH, ATTACK ANGLE = 0 DEGREES
 X .0336 IPA F Δ .0240 IPA F + .0120 IPA F \times .0030 IPA F \diamond .0030 IPA S
 \blacktriangle .0120 IPA S \square .0240 IPA S Y .0336 IPA S

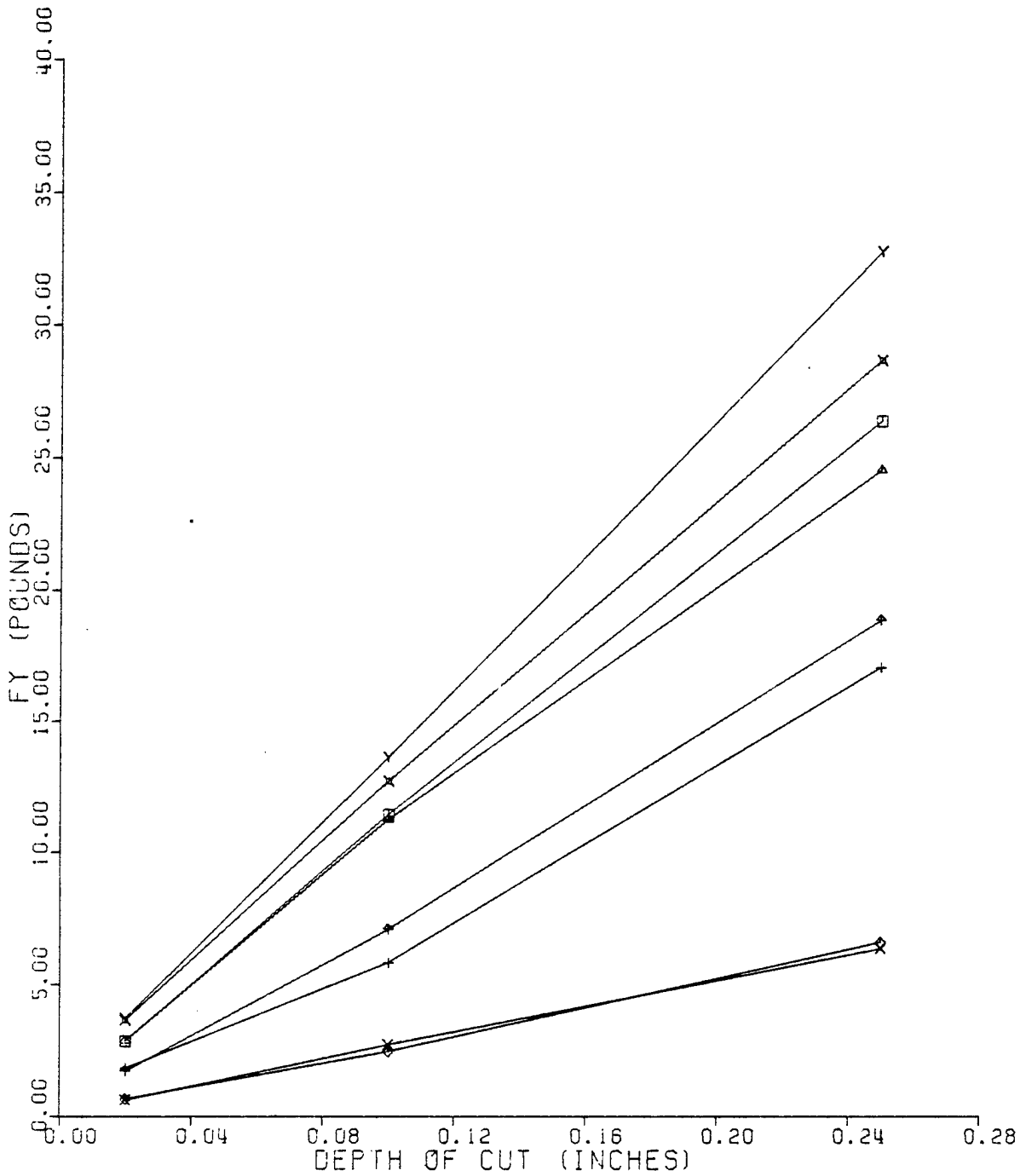


Fig. A-7. F_Y vs. Depth of Cut for LX-10 with 0.100 inch Radius Cutter

LX-10 TOOL FORCE STUDY F_Y VS DEPTH OF CUT
 CUTTER RADIUS = 0.250 INCH. ATTACK ANGLE = 0 DEGREES
 X .0336 IPR F Δ .0240 IPR F + .0120 IPR F × .0030 IPR F ◇ .0030 IPR S
 † .0120 IPR S □ .0240 IPR S Y .0336 IPR S

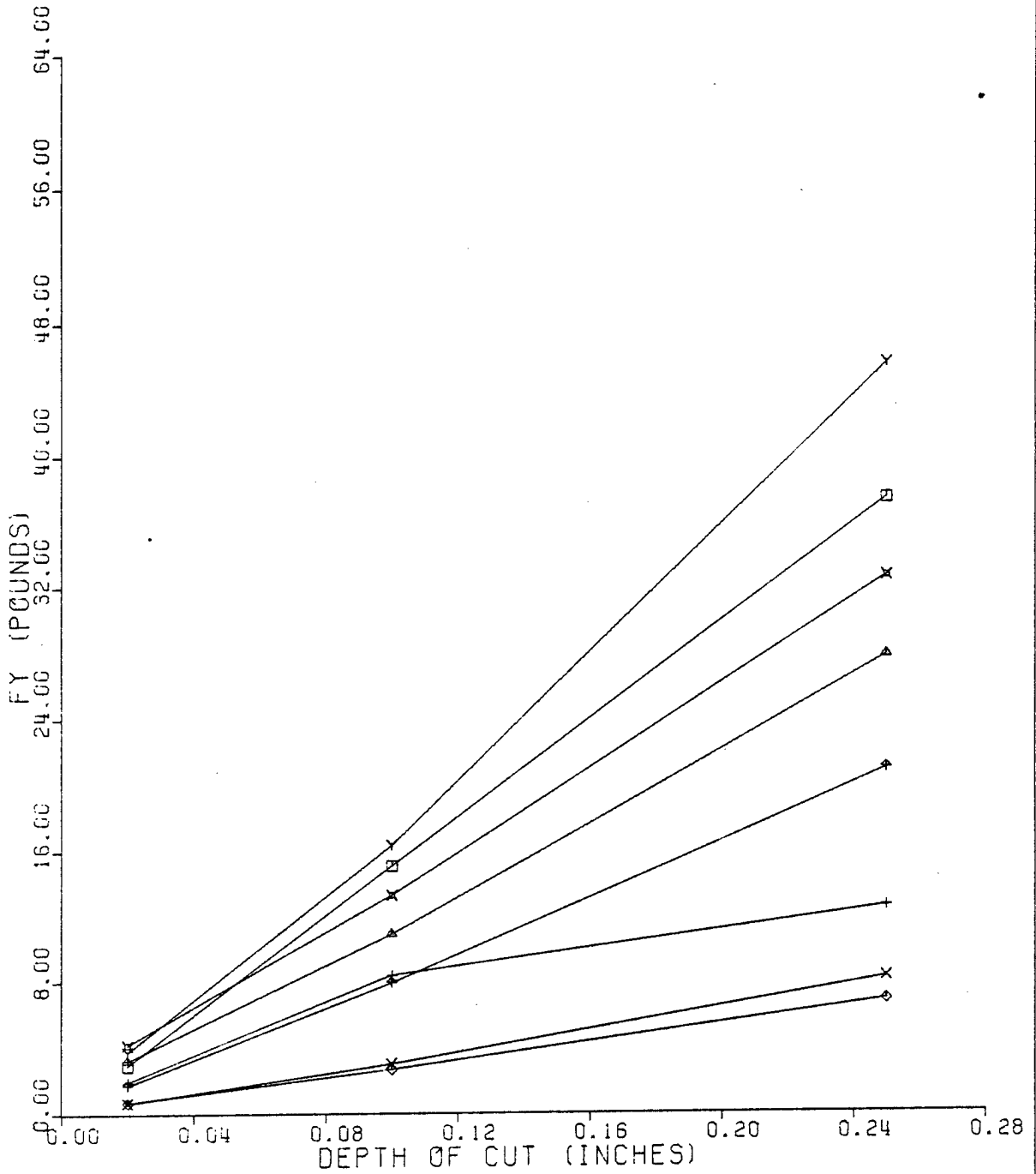


Fig. A-8. F_Y vs. Depth of Cut for LX-10 with 0.250 inch Radius Cutter

LX-10 TOOL FORCE STUDY FZ VS DEPTH OF CUT
 CUTTER RADIUS = 0.005 INCH, ATTACK ANGLE = 0 DEGREES
 X .0336 IPA F Δ .0240 IPA F + .0120 IPA F X .0030 IPA F ◇ .0030 IPA S
 † .0120 IPA S □ .0240 IPA S Y .0336 IPA S

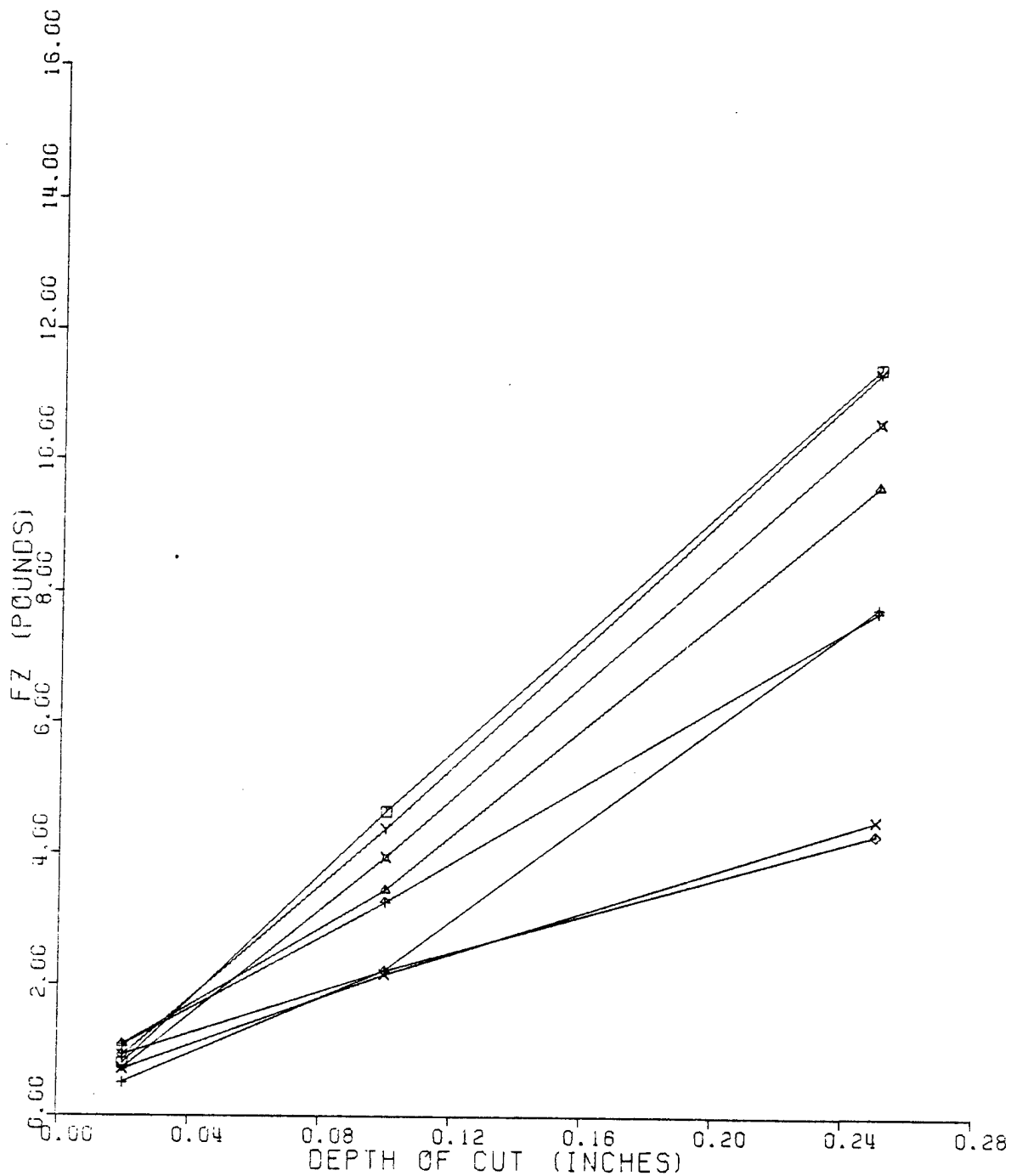


Fig. A-9. F_z vs. Depth of Cut for LX-10 with 0.005 inch Radius Cutter

LX-10 TOOL FORCE STUDY FZ VS DEPTH OF CUT
 CUTTER RADIUS = 0.030 INCH, ATTACK ANGLE = 0 DEGREES
 ✕ .0336 IPR F △ .0240 IPR F + .0120 IPR F ✕ .0030 IPR F ◇ .0030 IPR S
 † .0120 IPR S □ .0240 IPR S Y .0336 IPR S

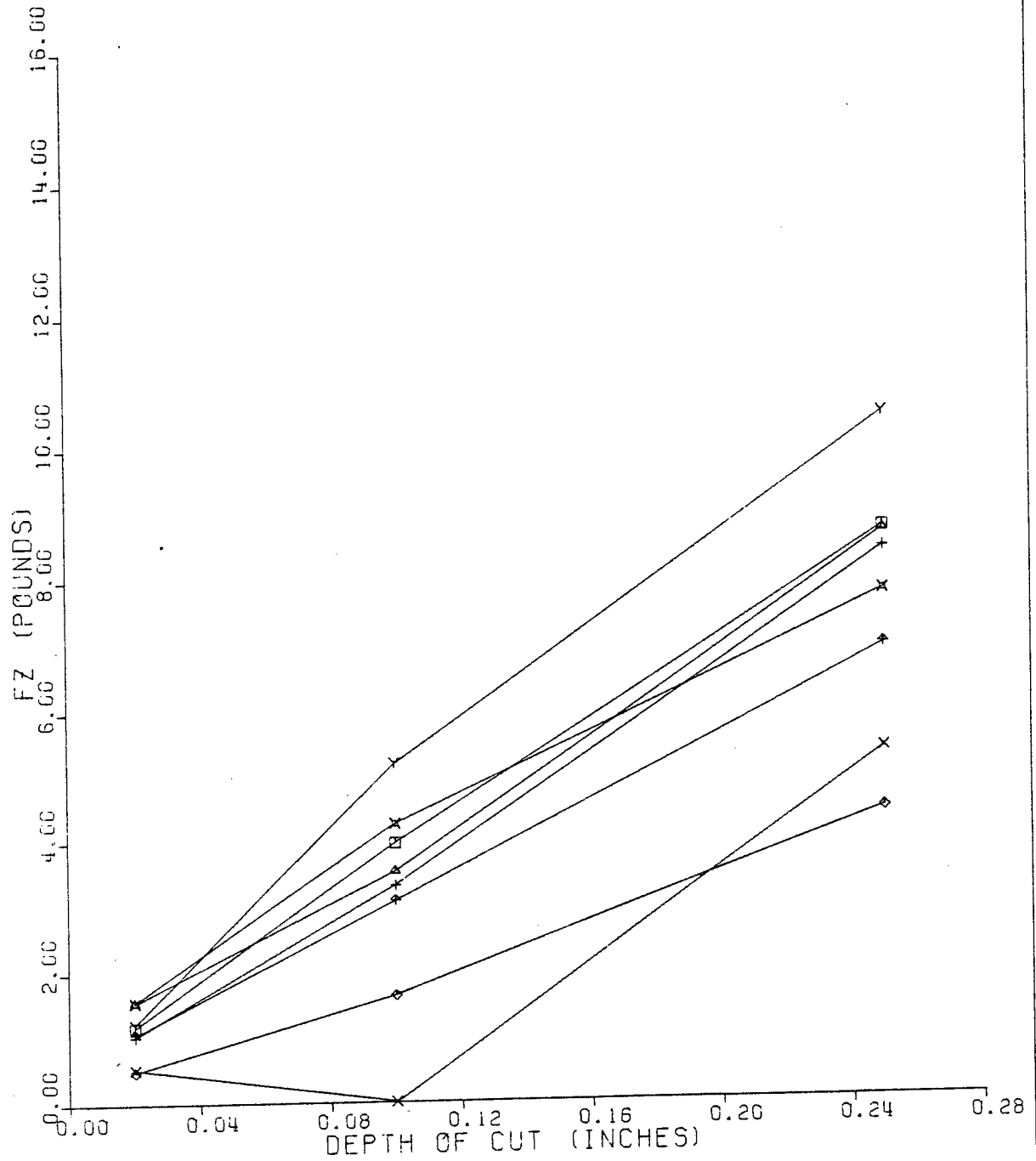


Fig. A-10. F_z vs. Depth of Cut for LX-10 with 0.030 inch Radius Cutter

LX-10 TOOL FORCE STUDY FZ VS DEPTH OF CUT
 CUTTER RADIUS = 0.100 INCH, ATTACK ANGLE = 0 DEGREES
 X .0336 IPA F Δ .0240 IPA F + .0120 IPA F × .0030 IPA F ◇ .0030 IPA S
 † .0120 IPA S □ .0240 IPA S Y .0336 IPA S

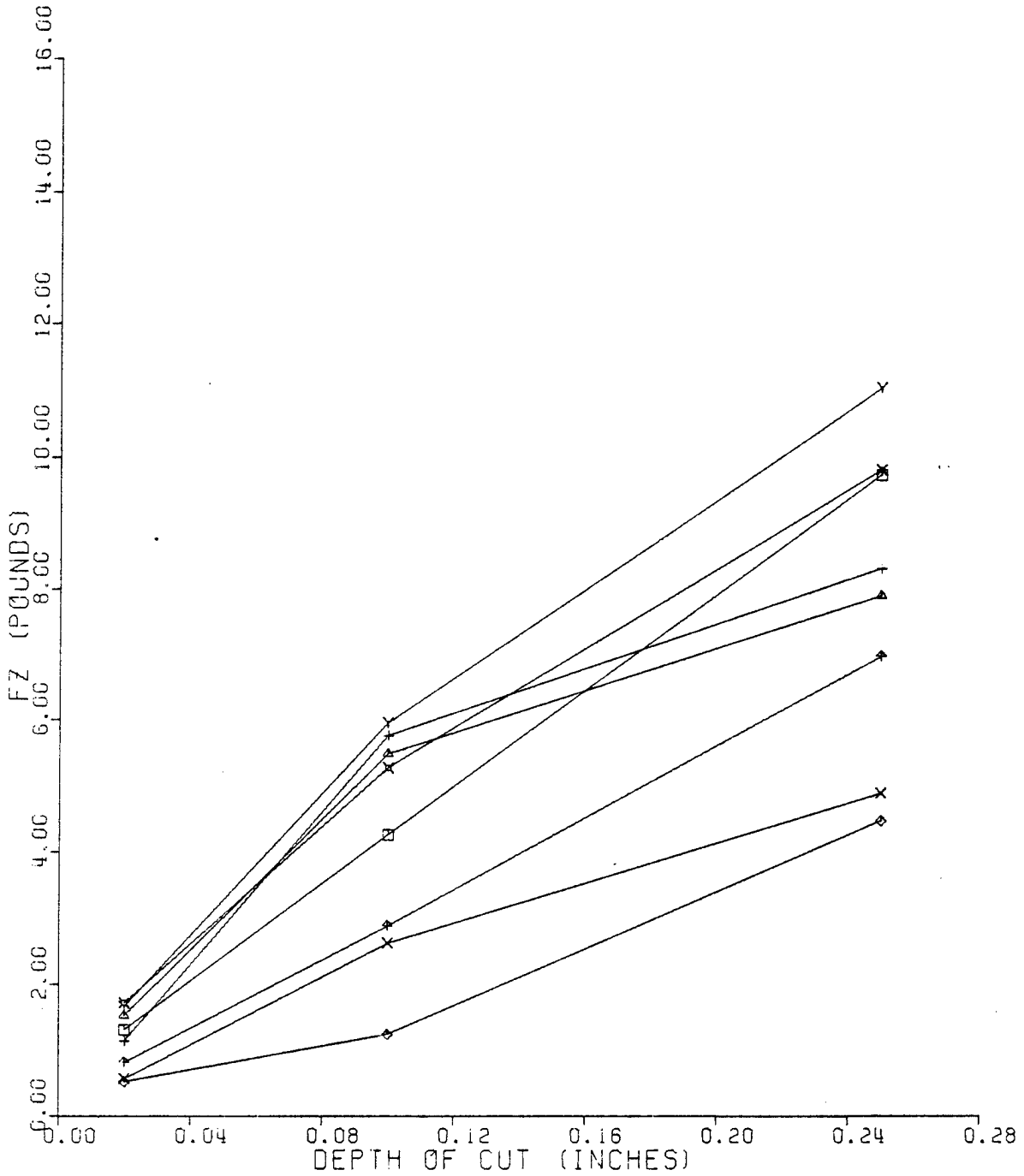


Fig. A-11. F_z vs. Depth of Cut for LX-10 with 0.100 inch Radius Cutter

LX-10 TOOL FORCE STUDY FZ VS DEPTH OF CUT
 CUTTER RADIUS = 0.250 INCH, ATTACK ANGLE = 0 DEGREES
 X .0336 IPRA F Δ .0240 IPRA F + .0120 IPRA F × .0030 IPRA F ◇ .0030 IPRA S
 † .0120 IPRA S □ .0240 IPRA S Y .0336 IPRA S

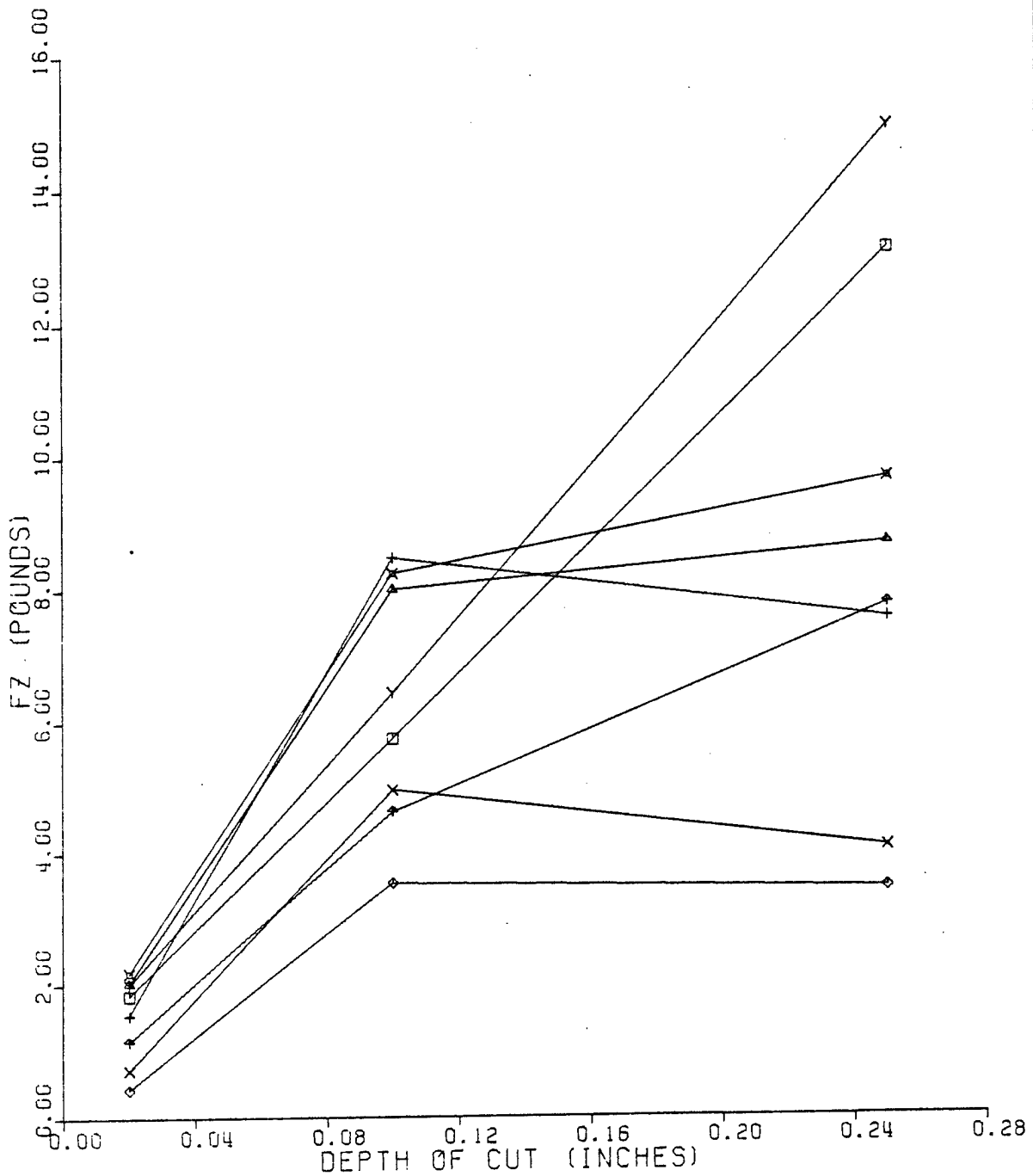


Fig. A-12. F_z vs. Depth of Cut for LX-10 with 0.250 inch Radius Cutter

LX-10 TOOL FORCE STUDY F_X VS CUTTER RADIUS
210 SFM AND 0.0336 IPR FEED

□ 0.250 DEPTH △ 0.100 DEPTH × 0.020 DEPTH

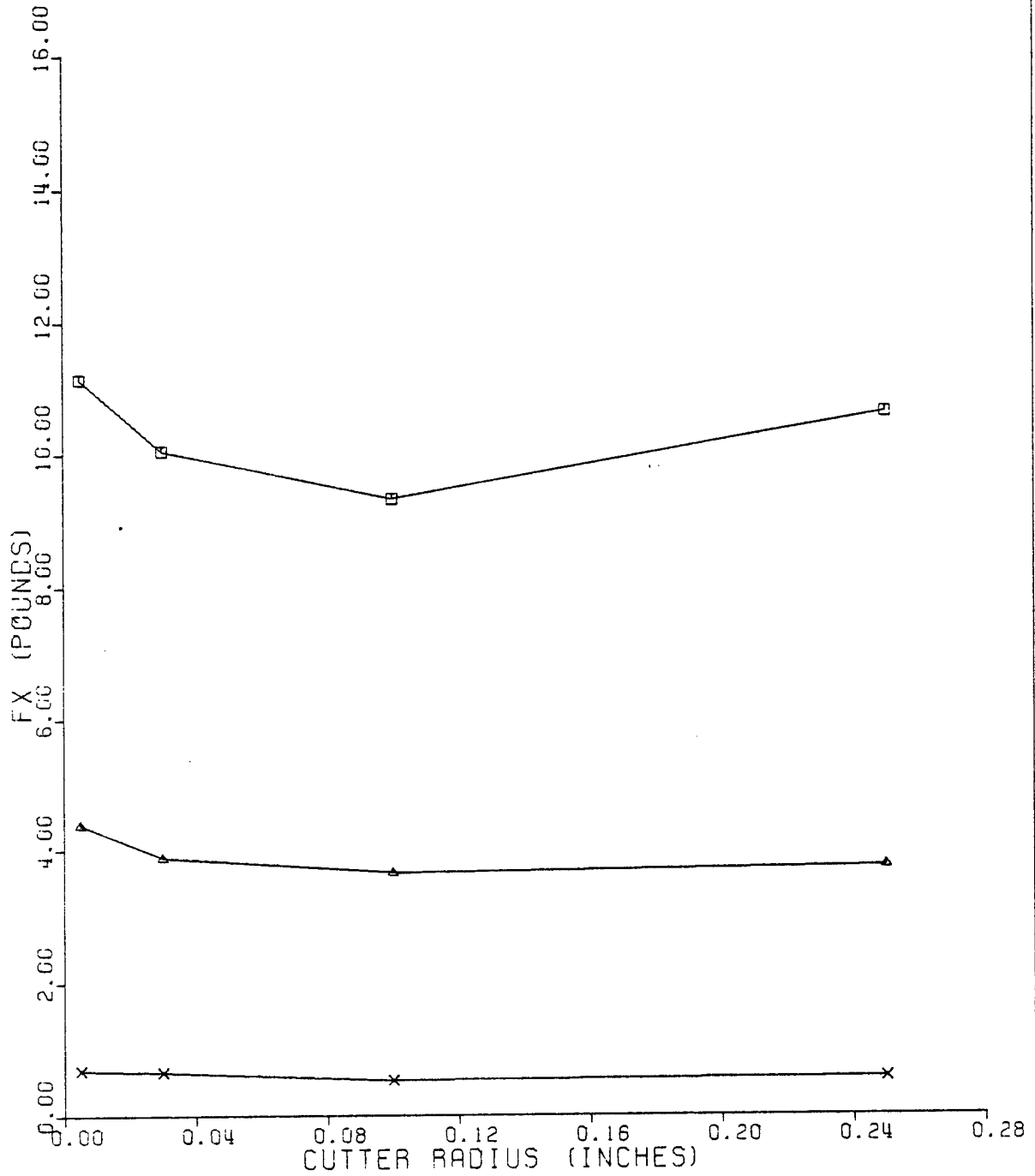


Fig. A-13. F_X vs. Cutter Radius for LX-10 at Different Cutting Depths

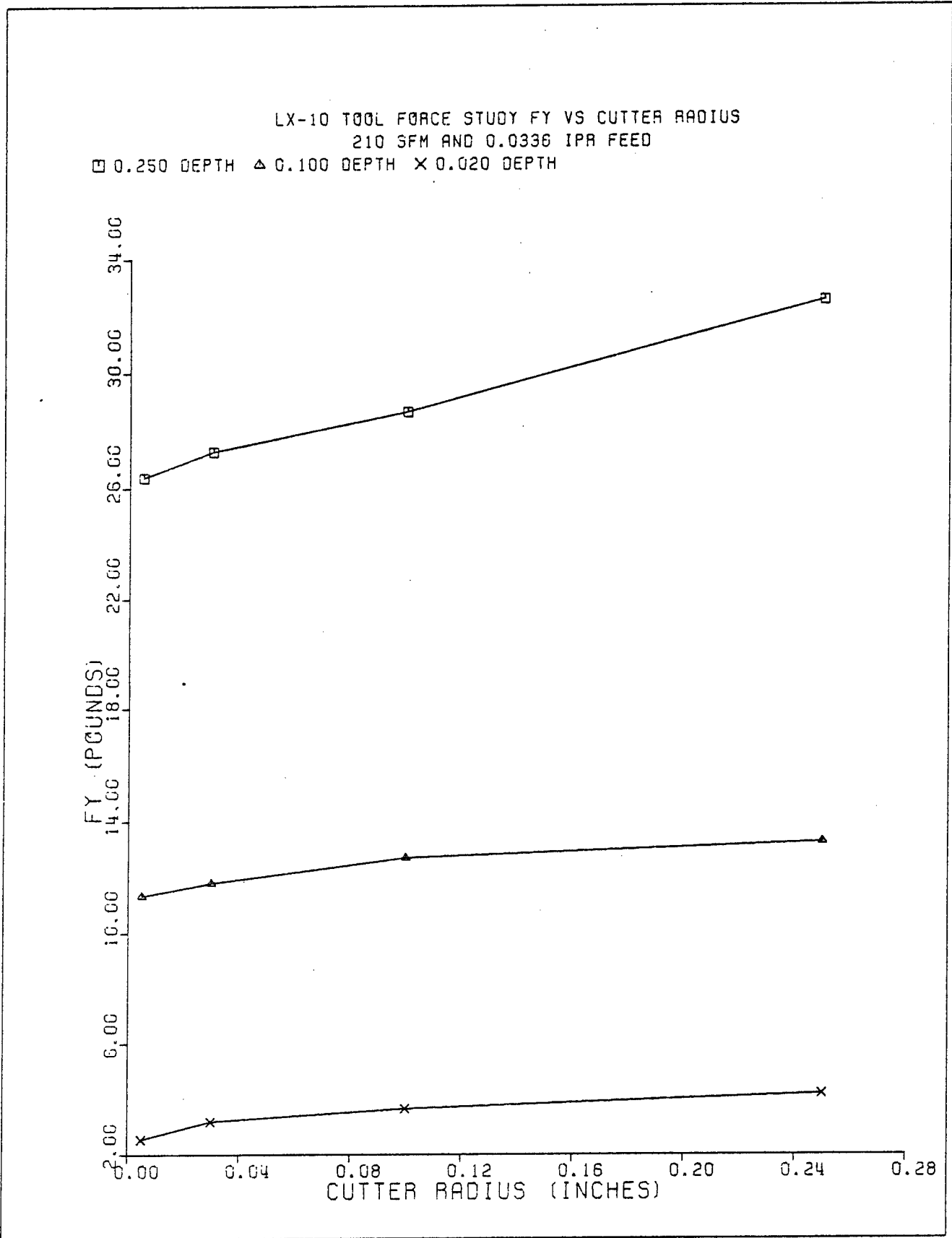


Fig. A-14. F_Y vs. Cutter Radius for LX-10 at Different Cutting Depths

LX-10 TOOL FORCE STUDY FZ VS CUTTER RADIUS

210 SFM AND 0.0336 IPA FEED

□ 0.250 RAD △ 0.100 RAD × 0.020 RAD

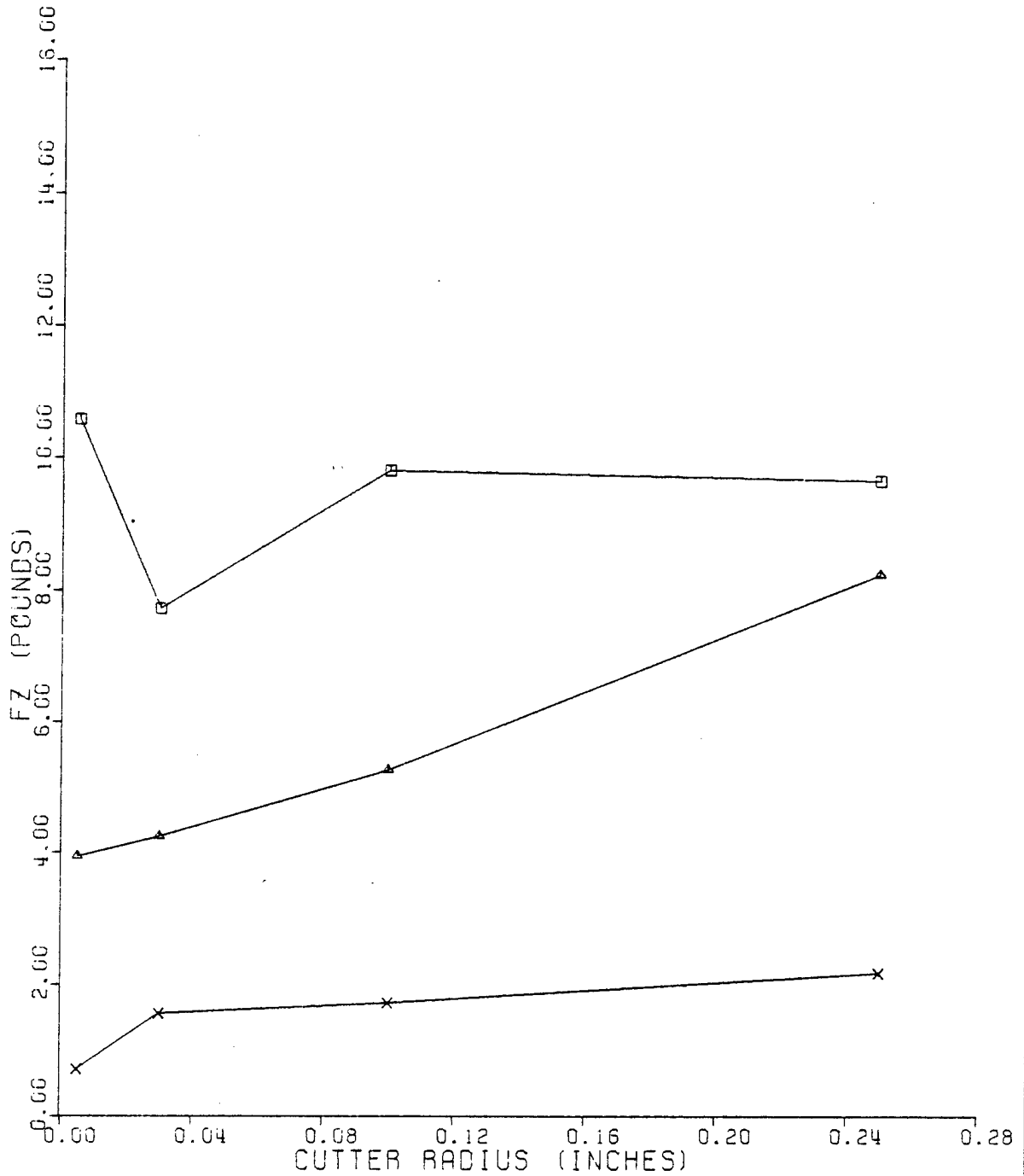


Fig. A-15. F_z vs. Cutter Radius for LX-10 at Different Cutting Depths

LX-10 TOOL FORCE STUDY F_X VS FEED RATE
 210 SFM, 0 DEG ATTACK, 0.250 DEPTH
 □ .250 RADIUS △ .100 RADIUS × .030 RADIUS † .005 RADIUS

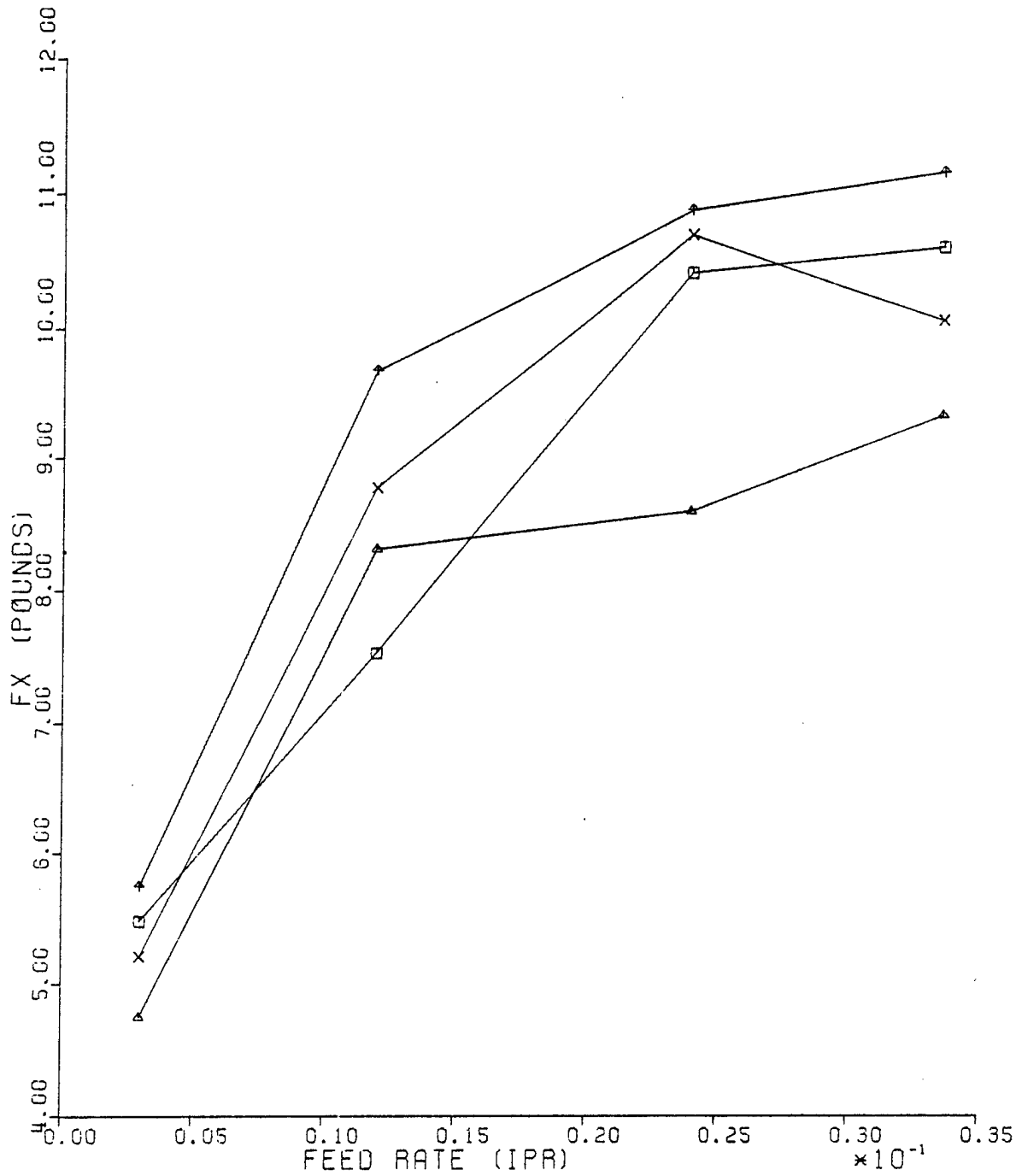


Fig. A-16. F_X vs. Feed Rate for LX-10 at Various Cutter Radii

LX-10 TOOL FORCE STUDY F_Y VS FEED RATE
 210 SFM, 0 DEG ATTACK, 0.250 DEPTH
 □ .250 RADIUS ▲ .100 RADIUS × .090 RADIUS ◆ .005 RADIUS

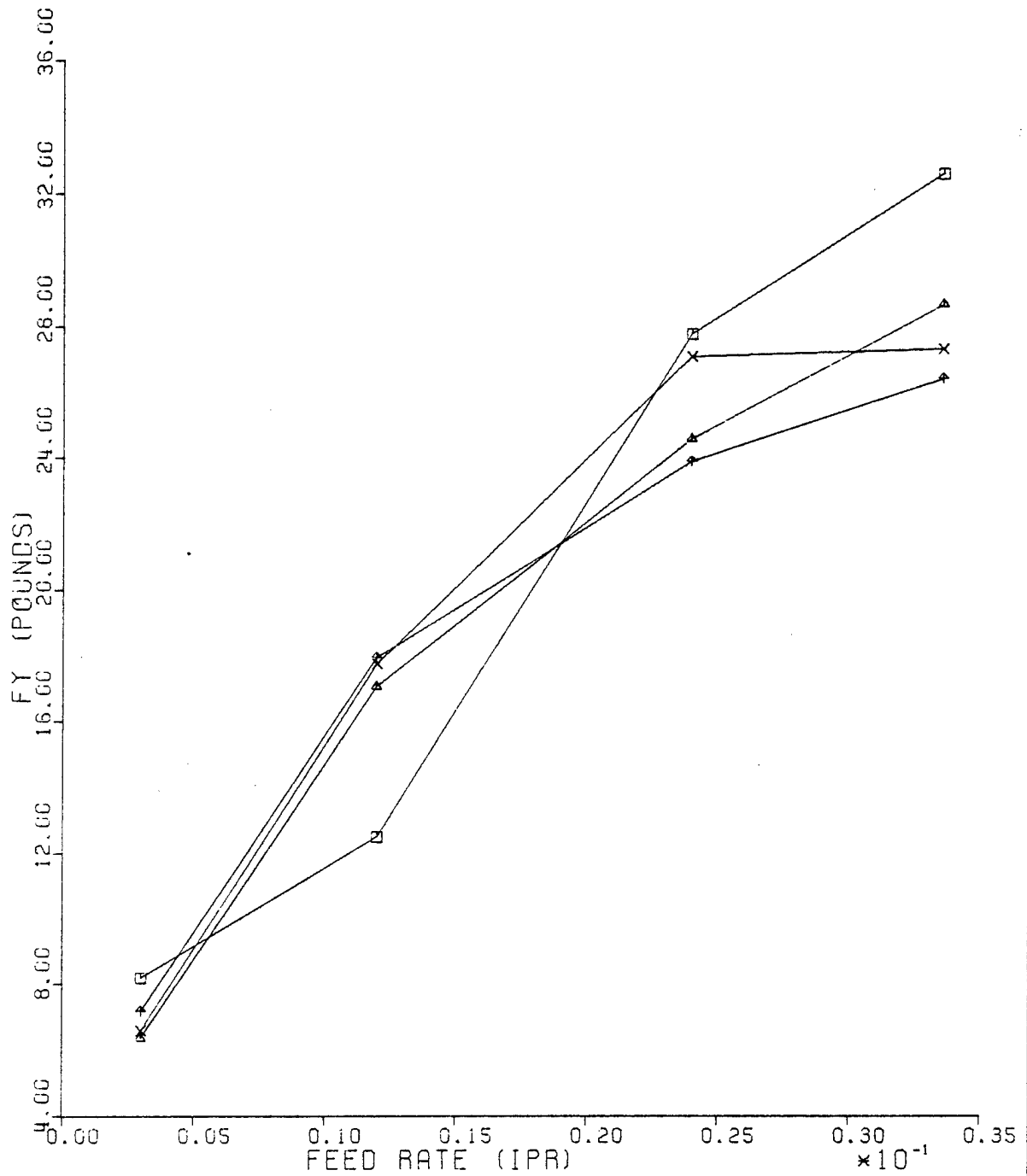


Fig. A-17. F_Y vs. Feed Rate for LX-10 at Various Cutter Radii

RX-03-BB TOOL FORCE STUDY F_X VS DEPTH OF CUT
 CUTTER RADIUS = 0.005 INCH. ATTACK ANGLE = 0 DEGREES
 X .0336 IPA F Δ .0240 IPA F + .0120 IPA F X .0030 IPA F \diamond .0030 IPA S
 \uparrow .0120 IPA S \square .0240 IPA S Y .0336 IPA S

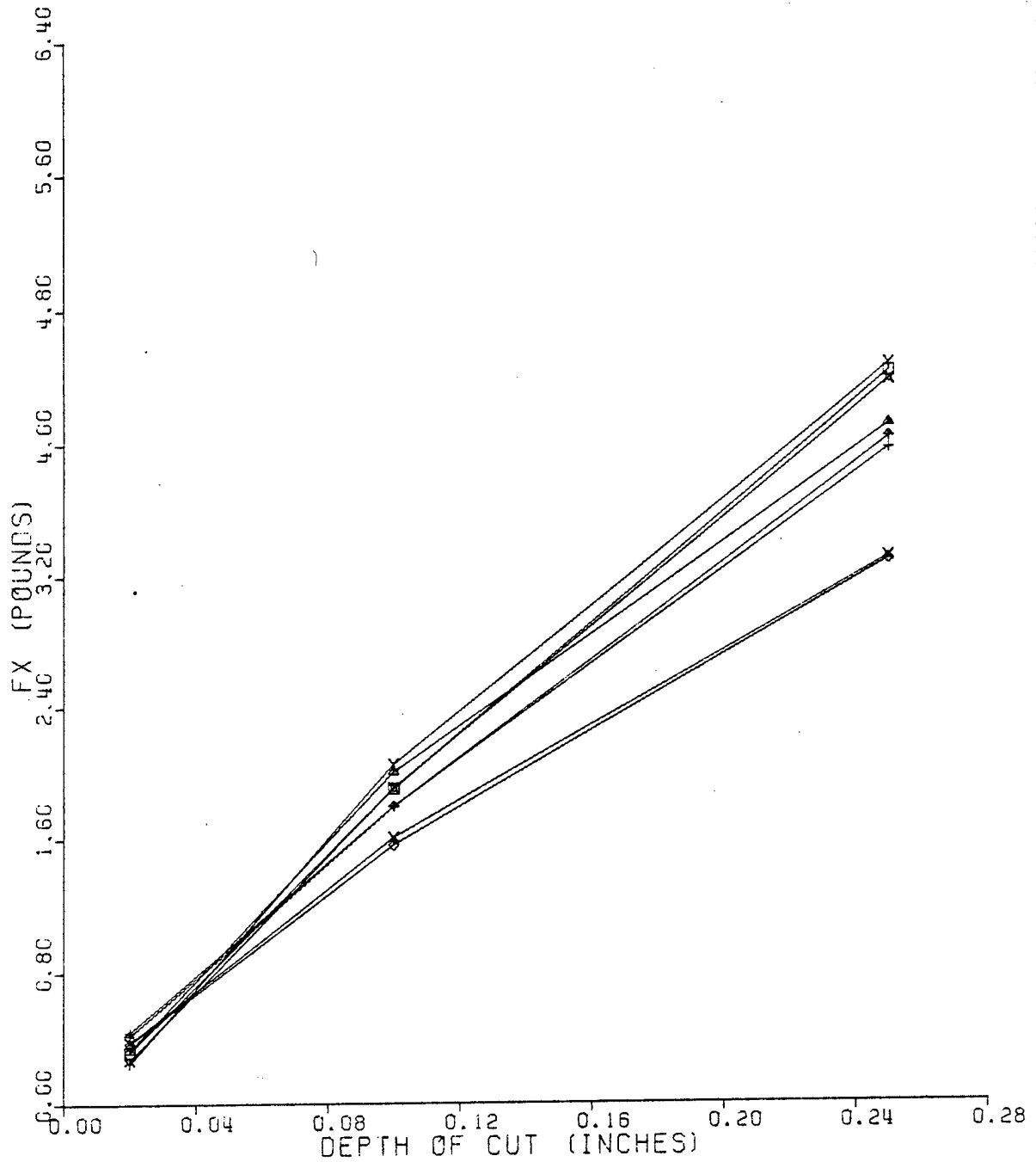


Fig. A-18. F_X vs. Depth of Cut for RX-03-BB with 0.005 inch Radius Cutter

RX-03-BB TOOL FORCE STUDY F_X VS DEPTH OF CUT
 CUTTER RADIUS = 0.030 INCH, ATTACK ANGLE = 0 DEGREES
 X .0336 IPR F Δ .0240 IPR F + .0120 IPR F X .0030 IPR F \diamond .0030 IPR S
 ∇ .0120 IPR S \square .0240 IPR S Y .0336 IPR S

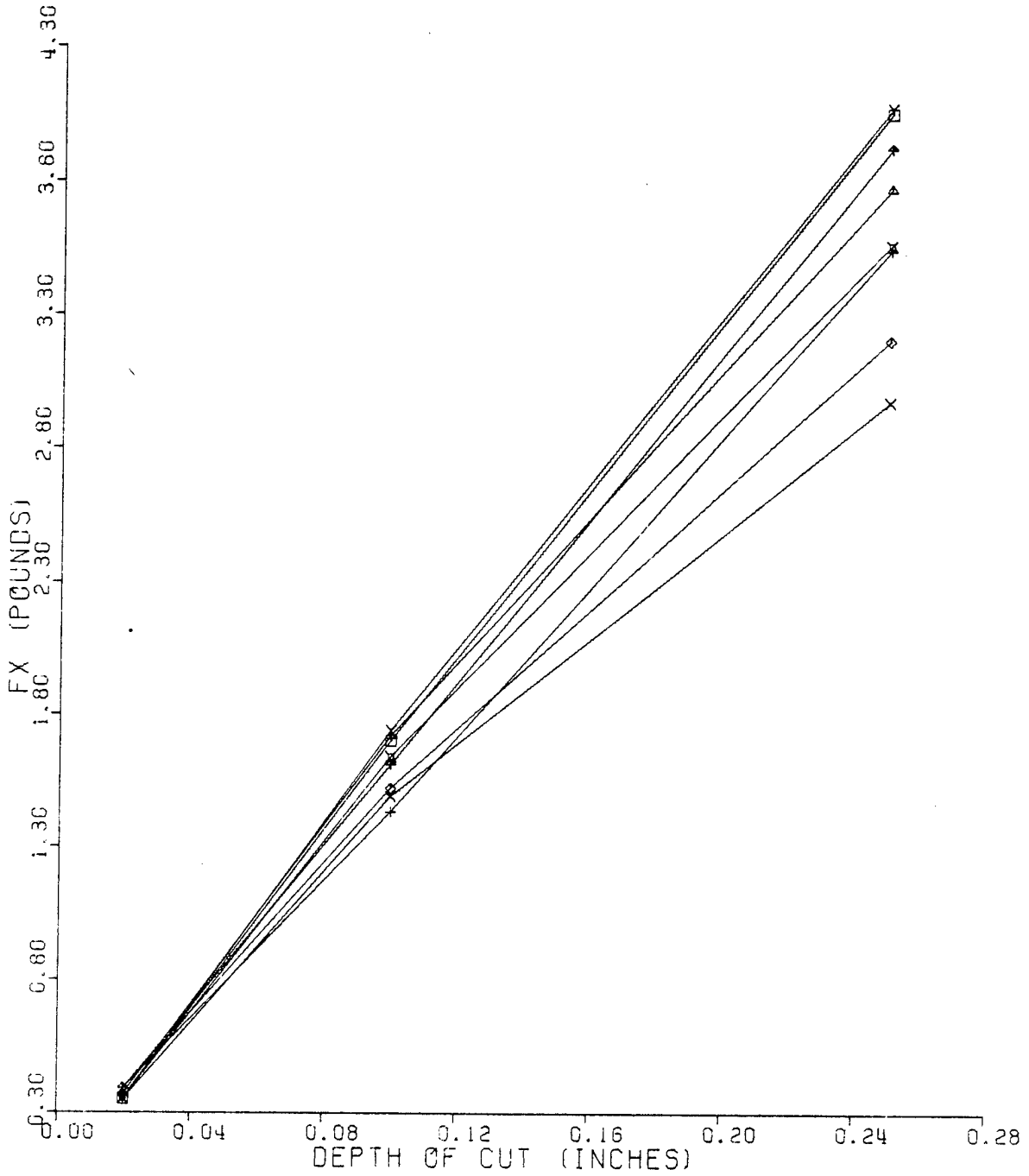


Fig. A-19. F_X vs. Depth of Cut for RX-03-BB with 0.030 inch Radius Cutter

RX-03-BB TOOL FORCE STUDY F_X VS DEPTH OF CUT
 CUTTER RADIUS = 0.100 INCH, ATTACK ANGLE = 0 DEGREES
 ✕ .0336 IPA F △ .0240 IPA F + .0120 IPA F ✕ .0030 IPA F ◇ .0030 IPA S
 † .0120 IPA S □ .0240 IPA S Y .0336 IPA S

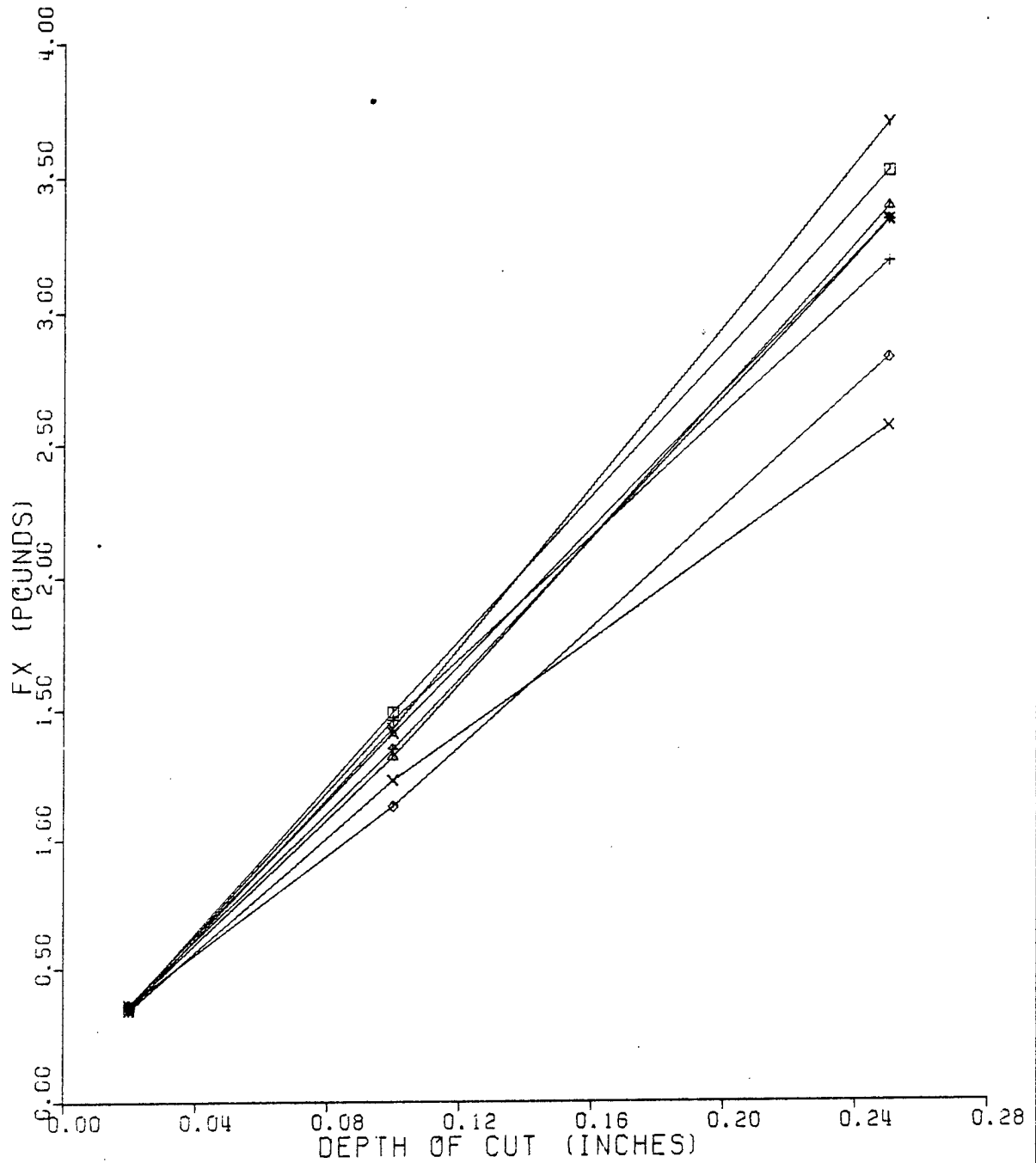


Fig. A-20. F_X vs. Depth of Cut for RX-03-BB with 0.100 inch Radius Cutter

RX-03-BB TOOL FORCE STUDY F_X VS DEPTH OF CUT
 CUTTER RADIUS = 0.250 INCH, ATTACK ANGLE = 0 DEGREES
 X .0336 IPR F Δ .0240 IPR F + .0120 IPR F X .0030 IPR F \diamond .0030 IPR S
 ∇ .0120 IPR S \square .0240 IPR S Y .0336 IPR S

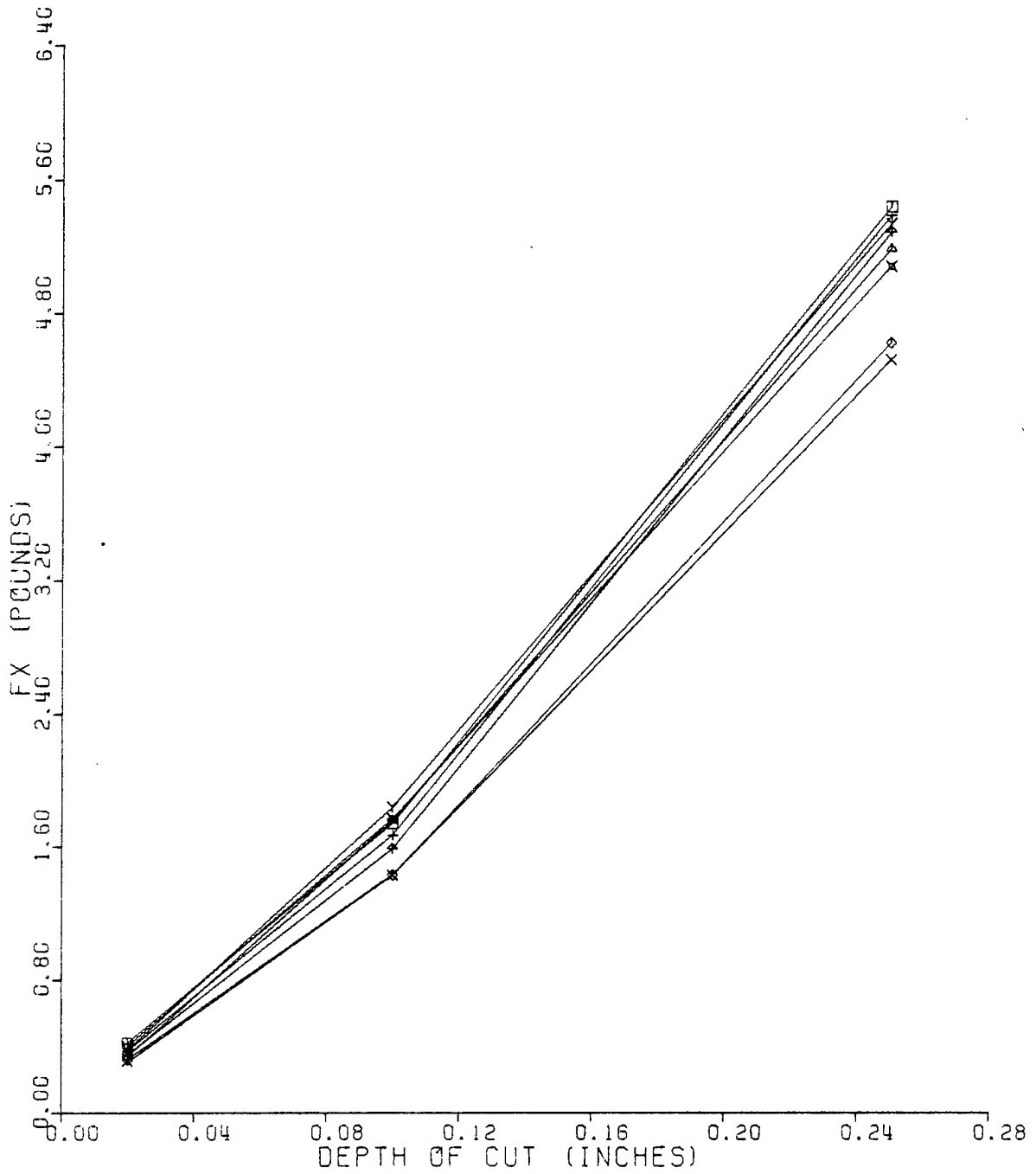


Fig. A-21. F_X vs. Depth of Cut for RX-03-BB with 0.250 inch Radius Cutter

RX-03-BB TOOL FORCE STUDY F_Y VS DEPTH OF CUT
 CUTTER RADIUS = 0.005 INCH, ATTACK ANGLE = 0 DEGREES
 X .0336 IPA F \blacktriangle .0240 IPA F + .0120 IPA F \times .0030 IPA F \diamond .0030 IPA S
 \blacktriangle .0120 IPA S \square .0240 IPA S Y .0336 IPA S

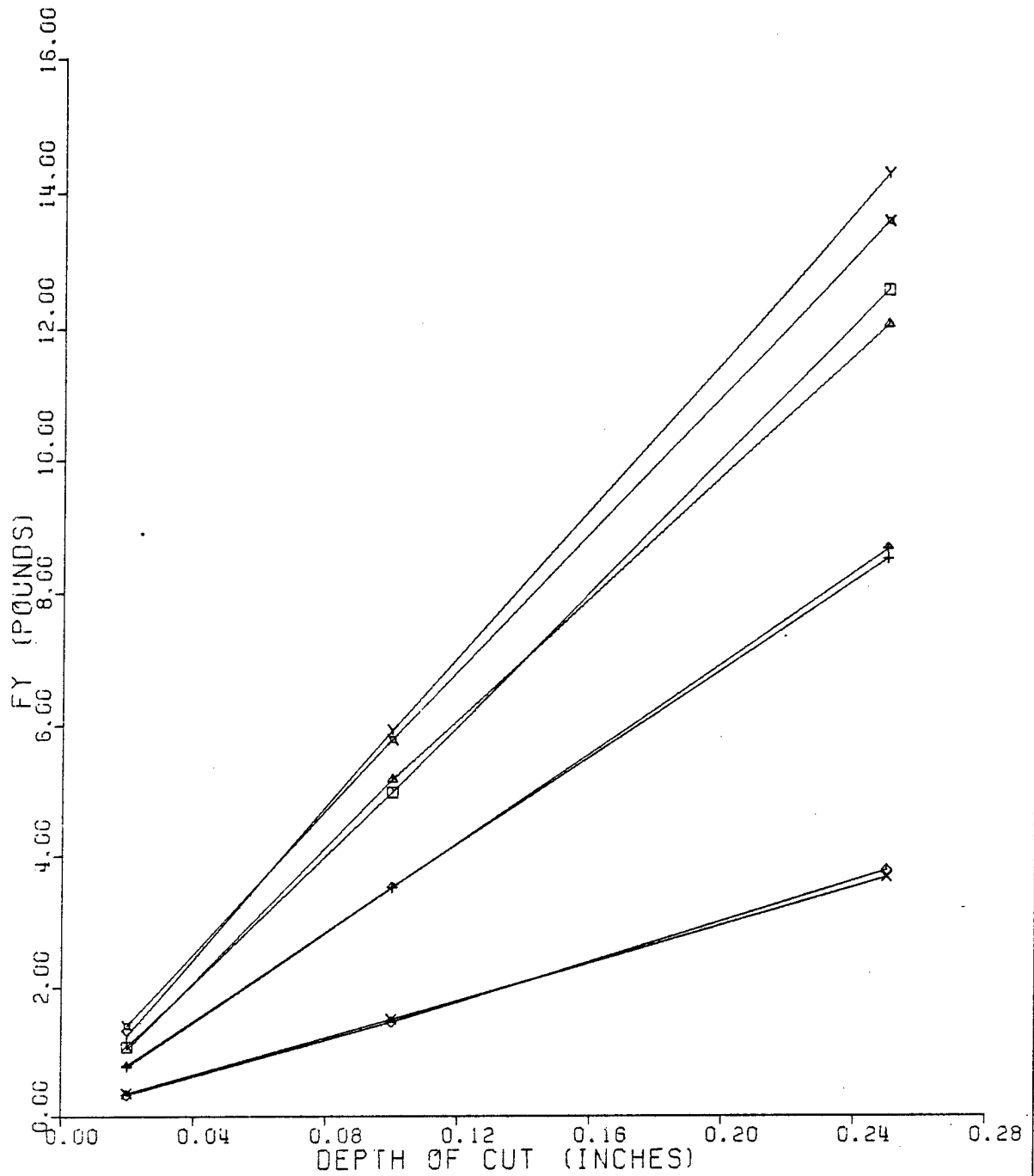


Fig. A-22. F_Y vs. Depth of Cut for RX-03-BB with 0.005 inch Radius Cutter

RX-03-BB TOOL FORCE STUDY F_Y VS DEPTH OF CUT
 CUTTER RADIUS = 0.030 INCH, ATTACK ANGLE = 0 DEGREES
 X .0336 IPR F Δ .0240 IPR F + .0120 IPR F × .0030 IPR F ◇ .0030 IPR S
 † .0120 IPR S □ .0240 IPR S Y .0336 IPR S

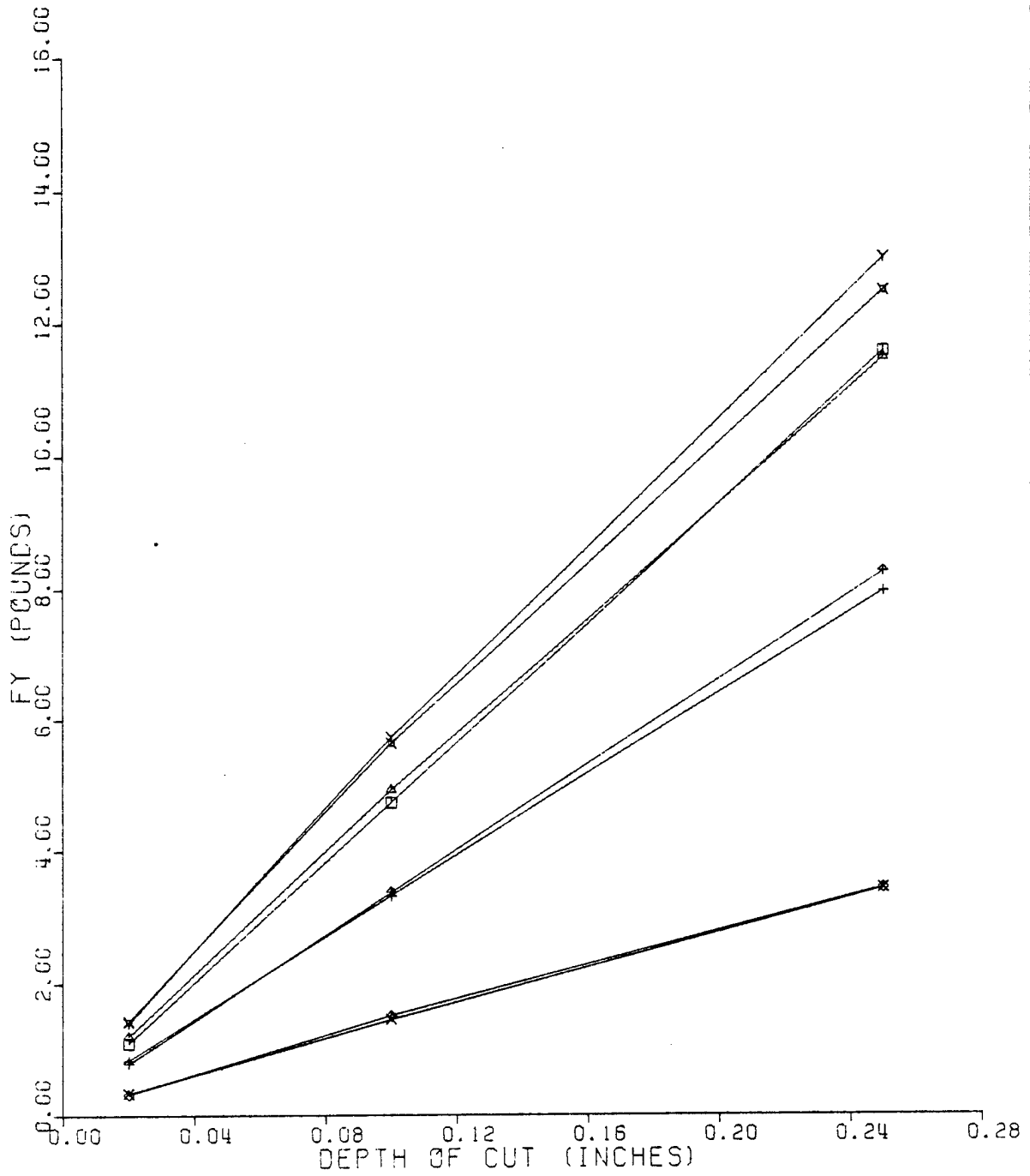


Fig. A-23. F_Y vs. Depth of Cut for RX-03-BB with 0.030 inch Radius Cutter

RX-03-BB TOOL FORCE STUDY F_Y VS DEPTH OF CUT
 CUTTER RADIUS = 0.100 INCH, ATTACK ANGLE = 0 DEGREES
 X .0335 IPA F Δ .0240 IPA F + .0120 IPA F X .0030 IPA F \diamond .0030 IPA S
 ∇ .0120 IPA S \square .0240 IPA S Y .0336 IPA S

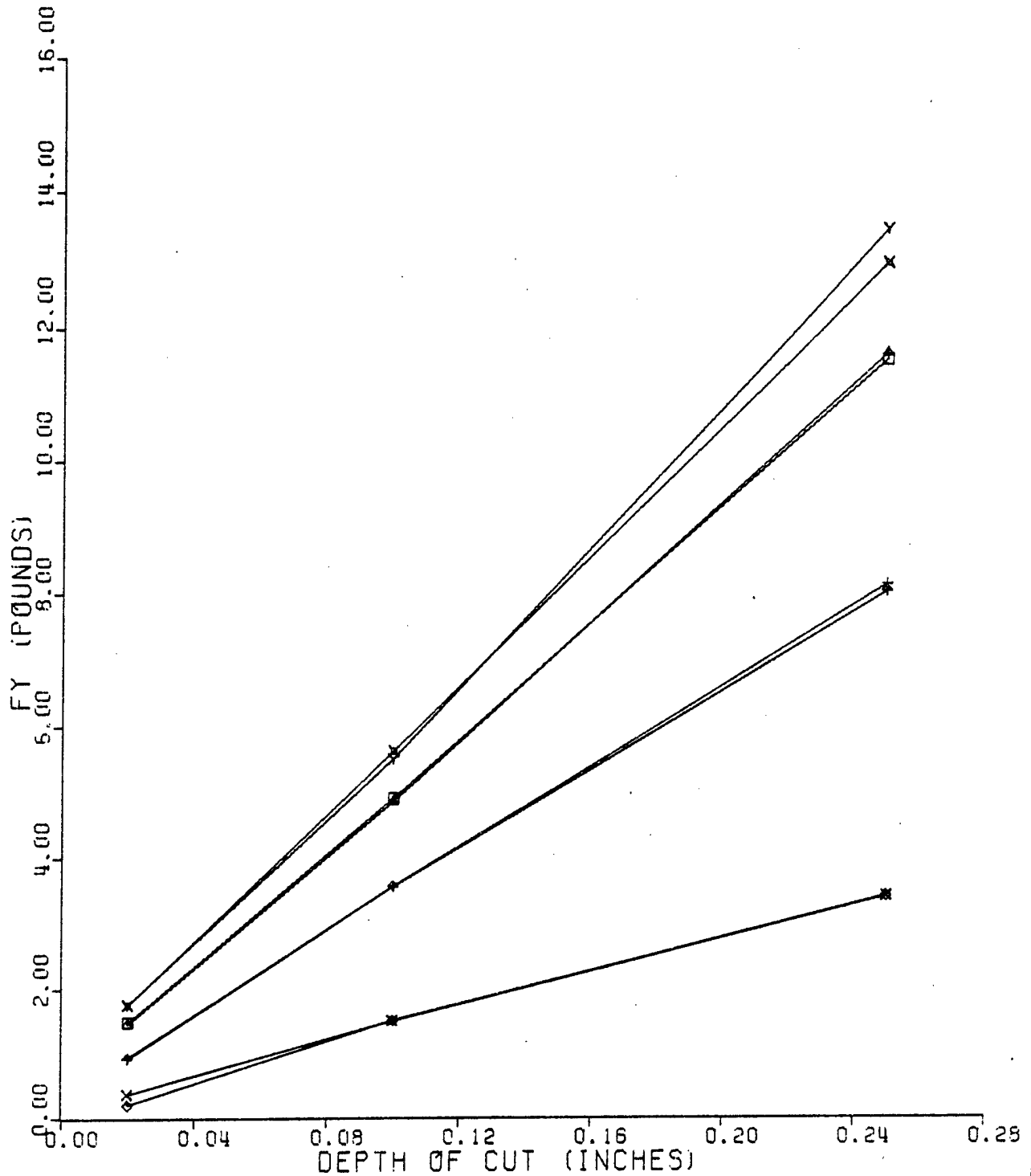


Fig. A-24. F_Y vs. Depth of Cut for RX-03-BB with 0.100 inch Radius Cutter

RX-03-BB TOOL FORCE STUDY F_Y VS DEPTH OF CUT
 CUTTER RADIUS = 0.250 INCH, ATTACK ANGLE = 0 DEGREES
 * .0336 IPR F △ .0240 IPR F + .0120 IPR F × .0030 IPR F ◇ .0030 IPR S
 † .0120 IPR S □ .0240 IPR S Y .0336 IPR S

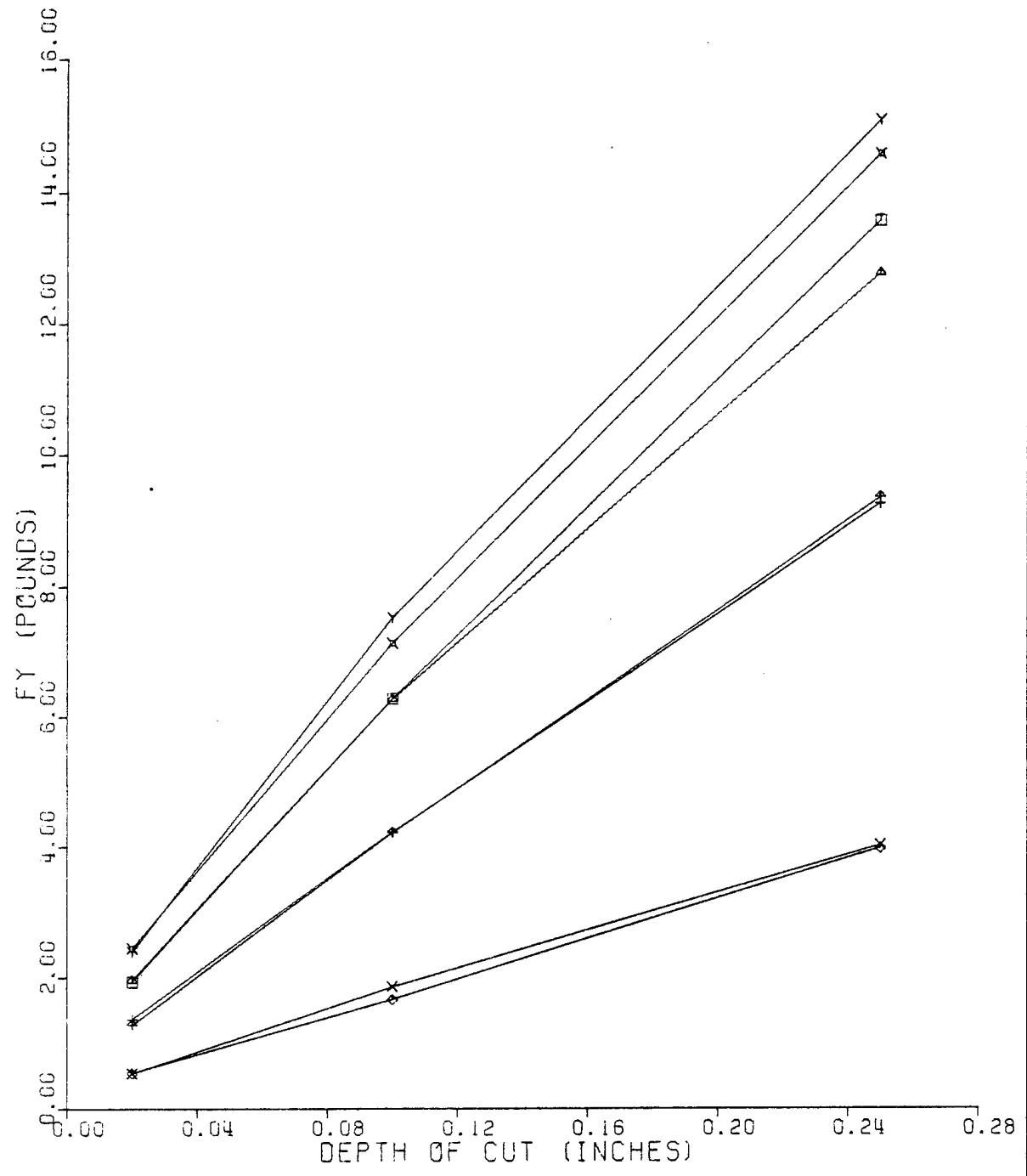


Fig. A-25. F_Y vs. Depth of Cut for RX-03-BB with 0.250 inch Radius Cutter

RX-03-BB TOOL FORCE STUDY F_X VS CUTTER RADIUS
150 SFM AND 0.0336 IPR FEED

□ 0.250 DEPTH △ 0.100 DEPTH × 0.020 DEPTH

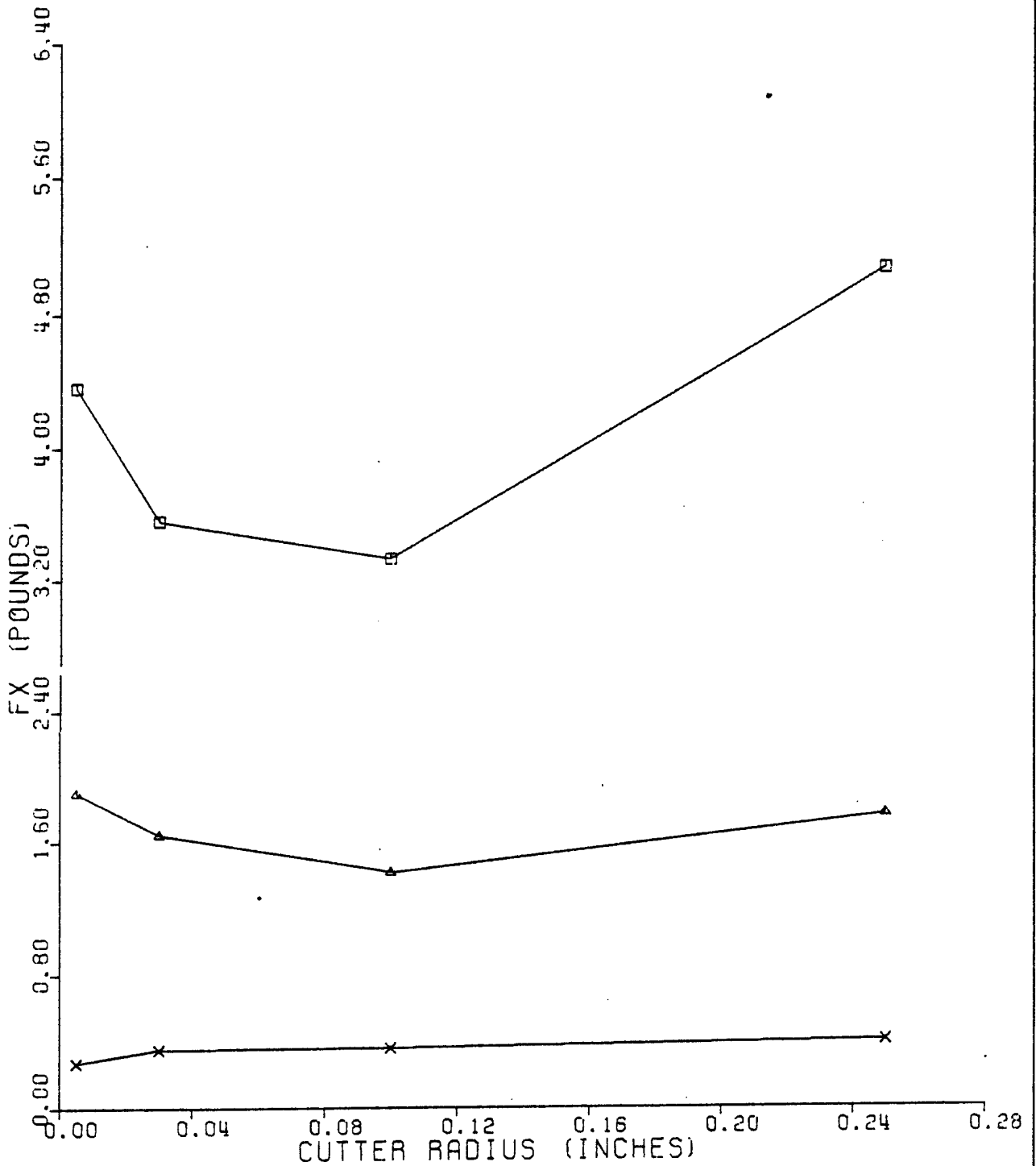


Fig. A-26. F_X vs. Cutter Radius for RX-03-BB at Different Cutting Depths

RX-03-BB TOOL FORCE STUDY F_Y VS CUTTER RADIUS
150 SFM AND 0.033G IPR FEED

□ 0.250 DEPTH ▲ 0.100 DEPTH × 0.020 DEPTH

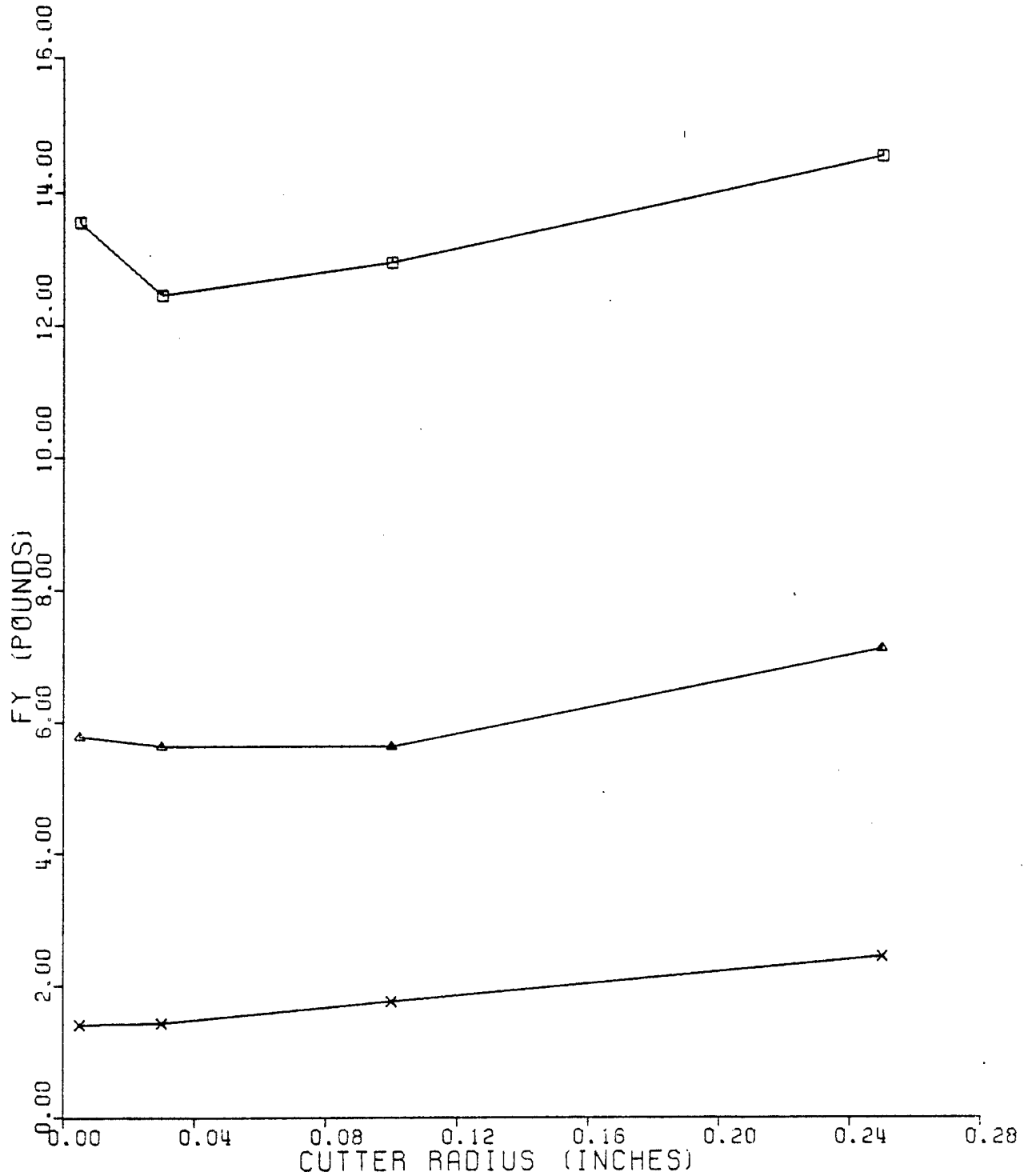


Fig. A-27. F_Y vs. Cutter Radius for RX-03-BB at Different Cutting Depths

RX-03-BB TOOL FORCE STUDY F_Y VS FEED RATE
 150 SFM, 0 DEG ATTACK, 0.250 DEPTH
 □ .250 RADIUS ▲ .100 RADIUS × .030 RADIUS † .005 RADIUS

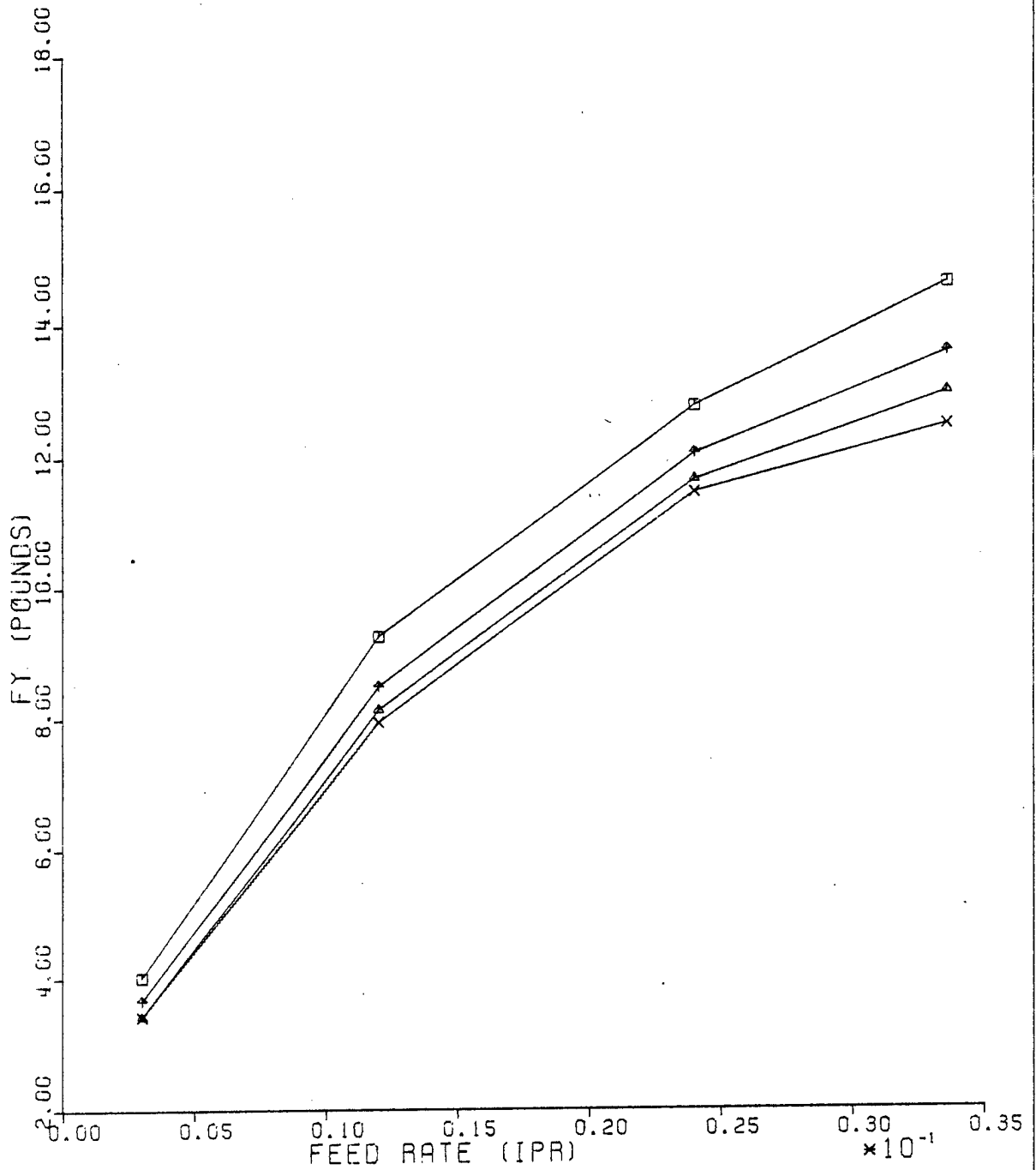


Fig. A-28. F_X vs. Feed Rate for RX-03-BB at Various Cutter Radii

RX-03-BB TOOL FORCE STUDY F_X VS FEED RATE
 150 SFM, 0 DEG ATTACK, 0.250 DEPTH
 □ .250 RADIUS △ .100 RADIUS × .030 RADIUS † .005 RADIUS

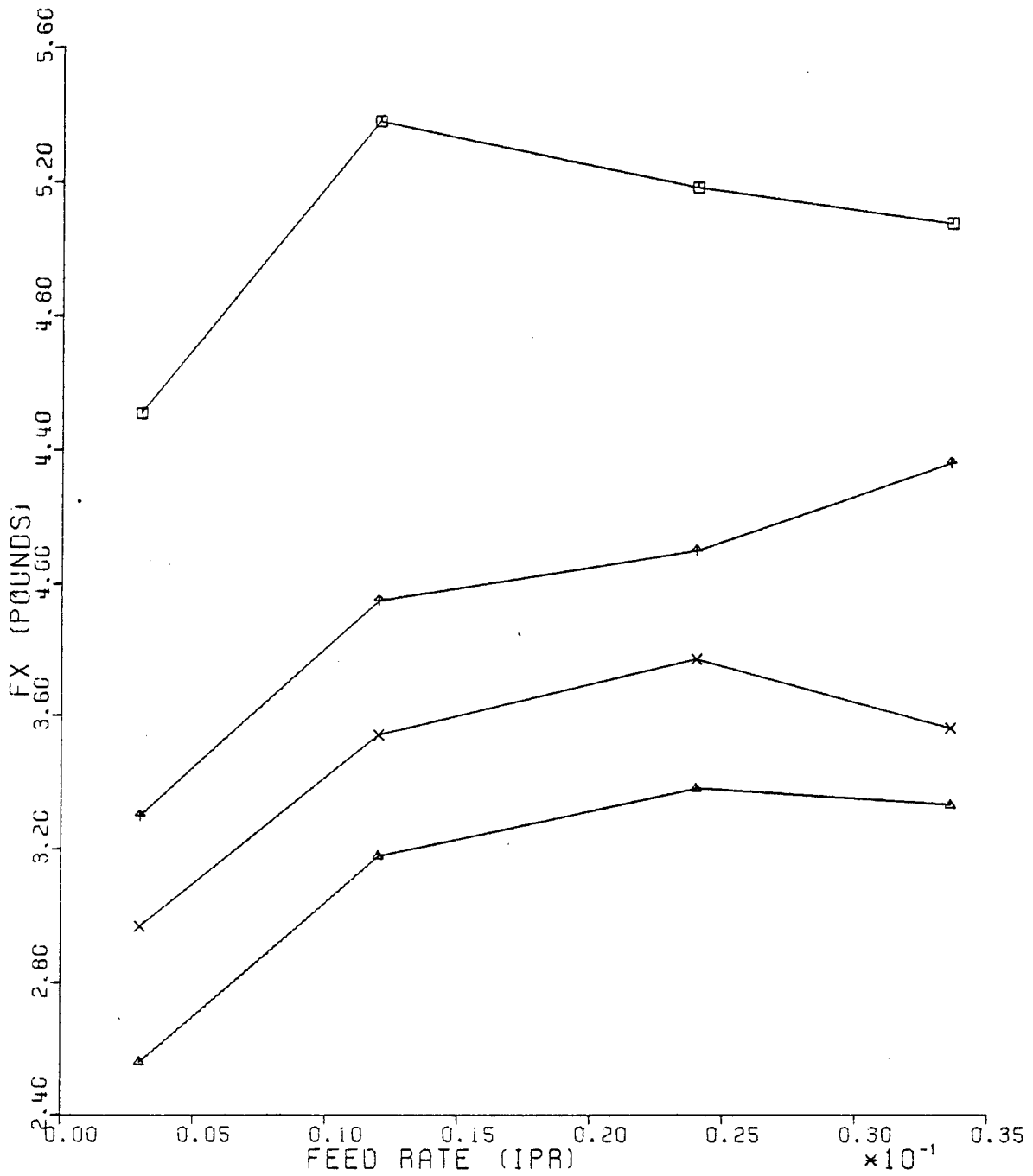


Fig. A-29. F_Y vs. Feed Rate for RX-03-BB at Various Cutter Radii

DISTRIBUTION

DOE

Ralph E. Caudle
Assistant Director of Operations
Military Application
Attn: Robert E. Clough
Washington, DC

ALO

H. N. Meyer, Director
Weapons Development Division

R. R. Fredlund, Jr., Director
Classification & Technical
Information

AAO

G. W. Johnson
Operations Branch

Mound Facility

R. T. Braun

SNLL

R. D. Cozine - Org. 8180

LLNL

G. S. Root (15 Copies)
Attn: A. C. Van Dyk

C. T. Brockett, Technical
Information Dept.

LANSL

E. H. Eyster - WX-DO
Attn: J. J. Wechsler

J. Aragon - WX-3

Report Library - ISD-4

SNLA

B. E. Arthur - Org. 4370

J. C. Crawford - Org. 2500/
D. H. Anderson - Org. 2510

C. B. McCampbell - Org. 2300

Central Technical Files - Org. 3141

TIC

Technical Information
Center (27 Copies)
Oak Ridge, TN

PX

Division Manager, Mfg. Engineering
Division Manager, Quality
Division Manager, Development
Division Manager, Manufacturing
Division Manager, Safety & Fire
Protection
Technical Library

Circulation Copy:

- (1) Plant Manager
- (2) M&H-SM Co., Inc., Lexington, KY